Exclusive Enteral Nutrition Initiates Individual Protective Microbiome Changes to Induce Remission in Pediatric Crohn's Disease

Häcker, Deborah[1,2]; Siebert, Kolja[3]; Smith, Byron J[4+]; Köhler, Nikolai[5]; Mahapatra, Aritra[6]; Heimes, Helena[1]; Metwaly, Amira[1]; Hölz, Hannes[3]; Manz, Quirin[8]; De Zen, Federica[3]; Heetmeyer, Jeannine[3]; Socas, Katharina[3]; Le Thi, Giang[3]; Meng, Chen[7]; Kleigrewe, Karin[7]; Pauling, Josch K[5]; Neuhaus, Klaus[6]; List, Markus[8]; Pollard, Katherine S[4,9,10]; Schwerd, Tobias[3&+]; Haller, Dirk[1,2,11&+]

[&]Authors contributed equally, [+]Corresponding author

[1] Chair of Nutrition and Immunology, TUM School of Life Sciences, Technische Universität München, Freising, Germany
[2] TUMCREATE, 1 CREATE Way, #10-02 CREATE Tower, Singapore 138602
[3] Department of Pediatrics, Dr. von Hauner Children's Hospital, University Hospital, LMU Munich, Germany.
[4] Gladstone Institutes, San Francisco, CA, USA
[5] LipiTUM, Chair of Experimental Bioinformatics, TUM School of Life Sciences, Technical University of Munich, Freising, Germany
[6] Core Facility Microbiome, ZIEL Institute for Food & Health, Technische Universität München, Freising, Germany
[7] Bavarian Center for Biomolecular Mass Spectrometry (BayBioMS), TUM School of Life Sciences, Technische Universität München, Freising, Germany
[8] Data Science in Systems Biology, School of Life Sciences, Technische Universität München, Freising, Germany
[9] University of California, San Francisco, CA, USA
[10] Chan Zuckerberg Biohub
[11] ZIEL Institute for Food & Health, Technische Universität München, Freising, Germany

Abstract

Exclusive enteral nutrition (EEN) is the first-line therapy for pediatric Crohn's disease (CD), but protective mechanisms remain unknown. We established a prospective pediatric cohort to characterize the function of fecal microbiota and metabolite changes of treatment-naïve CD patients in response to EEN. Integrated multi-omics analysis identified network clusters from individually variable microbiome profiles, with *Lachnospiraceae* and medium chain fatty acids as protective features. Metagenomic analysis identified high strain-level dynamics in response to EEN cessation, and hundreds of bacterial gene functions with significant changes in abundance. Functional changes of diet-exposed fecal microbiota were further validated in a combined approach using gut chemostat cultures and microbiota transfer into germ-free *Il10*-deficient mice. EEN-like and fiber-repleted dietary model conditions, respectively, induced individual strain signatures to prevent or cause IBD-like inflammation in gnotobiotic mice. Hence, we provide evidence that EEN therapy operates through explicit functional changes of temporally and individually variable microbiome profiles.

Keywords: Crohn's disease, pediatric, EEN, inflammatory bowel diseases, IBD, diet, fiber, fermentation, gut chemostat, FMT, data integration, microbiome, metabolome, microbial strains

Introduction

Crohn's disease (CD), one of the main entities of inflammatory bowel diseases (IBD), is a chronic and relapsing inflammatory condition of the gastrointestinal tract[1]. Epidemiological studies have demonstrated a significant increase in the incidence of CD in Westernized countries, particularly among the pediatric age group[2,3]. The pathogenesis of IBD involves host genetics and environmental influences, among which diet and the intestinal microbiome are key etiologic factors[4,5].

Exclusive enteral nutrition (EEN) is the first-line treatment for pediatric CD[6,7] and also shows efficacy in adult patients[8]. EEN refers to polymeric liquid formulas, which are mostly devoid of fibers[9]. Re-introducing regular diet after 6-8 weeks of EEN often results in recurrence of inflammation and disease activity[10]. EEN has been shown to drive changes in gut microbiota composition[11], but the high relapse rate after cessation of EEN suggests the presence of a CD-conditioned microbiome, which is able to re-establish after dietary intervention[12]. CD is associated with reduced bacterial diversity, compositional and functional changes, and the disruption of metabolic circuits between microbiome and host[13–15], however functional evidence for EEN-mediated changes in the microbiome as an underlying cause of therapeutic efficacy is still lacking.

Here, we identify EEN-protective signatures using integrated microbiota and metabolite analysis of treatment-naïve pediatric CD patients. Further, we functionally validate EEN-mediated protective changes in the microbiome using fecal microbiota transfer (FMT) from patients into *ex vivo* gut chemostat and germ-free (GF) *Il10*$^{-/-}$ mouse models. These systems allowed us to investigate the impact of diet on patient-derived fecal microbiota independent of the host, demonstrating that EEN directly shapes individual microbiomes to mediate protective functions in treatment-naïve CD patients.

Results

Microbiota and metabolite profiling identify individual responses to EEN therapy in pediatric CD patients

We established a pediatric IBD cohort and longitudinally followed 78 IBD patients (36 female, age at study inclusion 12.2 ± 3.9 years, 46 newly diagnosed) (**Fig. 1a, Extended Data Table 1**). Fecal samples from this cohort showed no clustering based on disease phenotype (CD, UC/IBDU) or EEN-exposure (**Fig. 1b, c,** 16S rRNA gene amplicon sequencing: 804 fecal samples [exposure antibiotics/probiotic n = 18/10] from 78 patients; untargeted metabolomic profiling: 467 fecal samples from 59 patients).

From the thirty-seven CD patients receiving EEN, we then focused explicitly on the 20 newly diagnosed and treatment naïve CD-EEN patients (**Fig. 1a, Extended Data Table 1**). At the end of EEN therapy, disease activity and inflammatory markers improved significantly, resulting in clinical response and induction of remission in 20/20 and 18/20 patients, respectively (**Fig. 1d**). During follow-up, patients received methotrexate (6/20), anti-TNF (13/20), or combination therapies (9/13) as maintenance treatment. Relapse after EEN was observed in 8/20 patients over one-year follow-up (**Fig. 1d**). Two patients switched from Modulen IBD® to Neocate Junior® during EEN due to suspected cow's milk protein allergy.

Analysis of samples before (PreEEN), during (EEN), and after EEN therapy (PostEEN) (microbiota profiling: 291 samples, metabolomic analysis: 145 samples) revealed patient-specific responses (**Fig. 1e, f and j**). Bacterial richness based on zOTUs (zero-radius operational taxonomic units) changed individually during formula feeding (**Fig. 1e, Extended Data Fig. 1a**), but was lower during active CD compared to remission (**Extended Data Fig. 1b, c**). Reminiscent of the total cohort, dendrograms of microbiota and metabolome analyses showed no EEN-specific clustering (**Fig. 1f, j**). Despite considerable overlap in multi-dimensional scaling (MDS) plots, microbial profiles were significantly different for: patients with active *vs*. inactive disease (**Fig. 1g**, n = 281, p = 0.001), during EEN intervention *vs*. PostEEN (**Fig. 1h,** n = 174**,** p-value = 0.001), and during early *vs*. late EEN exposure (**Fig. 1i**, n = 70, p-value = 0.017). PCA plots of metabolic profiles (**Fig 1k-m**) showed separation according to disease activity **(Fig 1k**), but weaker partitioning by diet (**Fig 1l**) and no separation by EEN duration (**Fig 1m**).

Integration of microbiota and metabolome data identifies key features of EEN exposure

Network analysis incorporating zOTU taxonomic profiles and untargeted metabolomics from 60 samples identified interlinked features, clustering in five distinct network communities (**Fig. 2a**). The communities with the highest performance in predicting EEN *vs*. PostEEN were identified (**Fig. 2b-d** based on Receiver Operating Characteristic (ROC)-Area under the Curve (AUC)) and the respective feature importance of the integrated data are displayed (**Fig. 2e-g**, Community 4 and 5 are shown in **Extended Data Fig. 2a, b**). In summary, we identified 16 zOTUs relevant for the integrated EEN signature and 9 zOTUs for the integrated PostEEN signature, including several zOTUs from the genera *Enterocloster* and *Clostridium* (formerly *Lachnoclostridium; Lachnospiraceae*) (**Fig. 2h, Extended Data Fig. 2c**). Most metabolites were predictive for PostEEN (n = 68), while 10 metabolites were linked to the protective effect of EEN (**Fig. 2e-g**, **Extended Data Fig. 2a, b** for Community 4 and 5). Of these, palmitoleic acid, lauric acid, decanoic acid and caprylic acid were identified as metabolite features present in Modulen IBD® (**Extended Data Fig. 2d**).

112 **Microbial strains and functions change dramatically at EEN cessation**

113 Next, we collected shotgun metagenomes for 96 CD-EEN patient samples (n = 19 patients) to
114 investigate the transition off of EEN. We detected 577 bacterial protein families with substantial
115 changes in abundance (45 increased and 532 decreased) at the transition off of EEN (**Fig. 3a**).
116 Families increased during EEN included COG3845 (mean log2 PostEEN/EEN of -0.68) and
117 COG4603 (-0.65), components of the ABC-type guanosine uptake system. Increases in
118 COG4813 (+1.67), annotated as trehalose utilization protein, and COG3867 (+0.98),
119 arabinogalactan endo-1,4-beta-galactosidase, indicate that microbes encoding these proteins
120 respond to host diet and may play a role in metabolite transformations. These findings are
121 consistent with changes in hexoses, disaccharides, and sugar acids found in the metabolite
122 analysis (**Fig. 2e-g**).

123 Computing the dissimilarity between pairs of samples from the same patient showed that
124 taxonomic turnover increased with time between samples (**Fig. 3b, c**). We observed
125 significantly more turnover in zOTU composition between pairs of samples across the
126 transition off of EEN ($p < 10^{-3}$ for both by permutation test) than during the EEN and PostEEN
127 time period (**Fig. 3b**). We next applied StrainFacts[16] to resolve taxonomic differences below
128 the level of species. Overall, we observed high strain-level diversity within and between CD-
129 EEN patients. For most of the 369 species, strains were largely specific to a single patient and
130 appeared in multiple samples from their host, while some samples contained multiple distinct
131 strains of a given species (**Supplementary Fig. 2**). We detected elevated strain turnover
132 during the transition off of EEN relative to the PostEEN period ($p < 10^{-3}$, **Fig. 3c**).

133 To further integrate 16S and metagenomic results, we identified pairs of zOTUs and
134 metagenomic species with relative abundance profiles that were highly correlated across
135 samples (e.g. **Fig. 3d**). This approach matched 26 zOTUs to one or more metagenomic
136 species (**Fig. 3e; Extended Data Table 2**), accounting for a median of 40% of relative
137 abundance per sample. Thus, metagenomics augmented amplicon sequencing, increased the
138 taxonomic resolution of our microbiome profiling, and revealed longitudinal dynamics in
139 microbial communities that was greatest at the transition off of EEN.

140 Next, we identified species with extensive strain turnover, large changes in relative abundance
141 at the end of EEN, high mean relative abundance, and high prevalence (**Fig. 3f**, **Extended**
142 **Data Table 3**, top 20). Using this composite score, we flagged 28 species as highly dynamic
143 and many of the top scoring species matched zOTUs (**Fig. 2**). Here we highlight the strain
144 dynamics of two closely related species, *Enterocloster bolteae* (formerly *Lachnoclostridium*
145 *bolteae*) and *E. clostridioformis* (formerly *C. clostridioforme*). Both of these metagenomic
146 species matched zOTU5 (**Fig. 3d, f**) and showed clear shifts in strain composition at or near

147 the transition off of EEN (**Fig. 3g, h**). In some patients, EEN and PostEEN samples contained
148 similar strains of each species, but the dominant strain changed; in others, a new strain
149 appeared PostEEN that was absent or undetectable during EEN. In contrast to *E.*
150 *clostridioformis*, the relative abundance of *E. bolteae* was significantly affected by EEN
151 cessation. Furthermore, while individual strains of this species did seem to respond to EEN
152 cessation, it had lower strain diversity and turnover overall (**Fig. 3h**). This distinction among
153 strains and between closely related species reinforces the importance of strain-level
154 characterization in individuals.

155 Altogether, metagenomic analyses demonstrate that gut microbial communities are dynamic
156 at and below the species level and highly influenced by EEN, motivating us to explore their
157 relationship to the clinical efficacy of EEN.

158 **EEN-like diet triggers protective changes in fecal microbiota**

159 To further evaluate the functional impact of EEN on patient-derived fecal microbiota, we used
160 continuous culture systems in a gut chemostat model and fecal microbiota transfer (FMT) into
161 GF WT and *Il10*$^{-/-}$ mice. *Il10*$^{-/-}$ mice are a microbiota-dependent IBD mouse model responsive
162 to human fecal microbiota, as previously shown for adult CD patients[17] (**Fig. 4a**). We selected
163 fecal samples from model patients (MP) at different disease states and response to therapy
164 (**Fig. 4b, c, i**).

165 Microbiota transfer of the PreEEN sample of MP1 (MP1-FMT 1, **Fig. 4b,** red arrow) induced
166 colonic tissue inflammation in all gnotobiotic *Il10*$^{-/-}$ mice (histopathology score of 5.3 ± 1.0) but
167 not in WT control mice (**Fig. 4d** p = 0.002, histopathology score of 1.3 ± 0.5; **Supplementary**
168 **Fig. 3a** H&E), mirroring the active disease state of this patient. Following transfer of MP1 fecal
169 material into the gut chemostat model (MP1-FMT 2, **Fig 4a**), dietary exposure was mimicked
170 using combinations of fiber-free EEN-like and fiber-repleted (FR) medium, respectively
171 (**Extended Data Fig. 3a, b**). We then transferred microbiota (MP1-FMT 3) from the chemostat
172 model exposed to EEN-like medium and thereby reversed the inflammatory phenotype of MP1
173 in *Il10*$^{-/-}$ mice (**Fig. 4d**, histopathology score of *Il10*$^{-/-}$ mice = 2.5 ± 0.8; WT mice = 1.6 ± 0.5;
174 **Fig. 4f**, H&E, **Supplementary Fig. 3a**). Conversely, under fiber-repleted medium conditions
175 MP1-FMT 4 induced IBD-like tissue pathology in four out of six *Il10*$^{-/-}$ mice (**Fig. 4d**
176 histopathology score = 3.7 ± 1.0; **Fig. 4f** H&E, **Supplementary Fig. 3a**), compared to disease-
177 free WT mice (**Fig. 4d** histopathology score = 1.4 ± 0.5, p = 0.0087; **Fig. 4f** H&E,
178 **Supplementary Fig. 3a**). *Tnf* gene expression confirmed active tissue inflammation with
179 significantly elevated expression levels in *Il10*$^{-/-}$ compared to WT mice (**Fig. 4f** p = 0.0022 dist.
180 colon; **Supplementary Fig. 3d** p = 0.0152 prox. colon). Thus, *ex vivo* EEN-like intervention
181 recapitulated therapeutic functional changes to the microbiota.

182 Transfer of the fecal microbiota from MP2 failed to induce inflammation in *Il10*$^{-/-}$ mice (MP2-
183 FMT 1, **Fig 4e** H&E, **Supplementary Fig. 3b**), resembling the inactive disease state of the
184 patient. Since the stool sample of MP2 was retrieved under EEN therapy, we started the gut
185 chemostat on EEN-like medium (MP2-FMT 2; **Extended Data Fig. 3c**). In contrast to MP2-
186 FMT 3 (**Fig. 4e** histopathology score in in *Il10*$^{-/-}$ = 2.0 ± 0.6; WT = 1.0 ± 0.6; **Fig. 4g** H&E**,**
187 **Supplementary Fig. 3b**), transfer of FR-conditioned microbiota (MP2-FMT 4) triggered IBD-
188 like colitis, including histopathologic changes and elevated *Tnf* tissue expression (**Fig. 4e**,
189 histopathology score in *Il10*$^{-/-}$ = 4.8 ± 1.9 *vs*. WT = 1.5 ± 0.5, p = 0.0152; **Fig. 4g** H&E, *Tnf* gene
190 expression p = 0.0152 dist. colon; **Supplementary Fig. 3d** p = 0.0022 prox. colon). Thus, both
191 transfer experiments (MP2-FMT 1 and MP2-FMT 3) demonstrate protective effects of EEN.
192 Reintroduction of fiber (MP2-FMT 4) reverted this protective function, indicative for the risk of
193 relapse in MP2 after EEN cessation (**Fig. 4c**).

194 Next, we introduced an EEN-like mouse diet one week prior to FMT (MP3-FMT 4) to evaluate
195 extended dietary effects in gnotobiotic WT and *Il10*$^{-/-}$ mice (**Fig. 4h**). MP3 had elevated fecal
196 calprotectin levels of 2828 mg/L (**Fig. 4i**, blue arrow) and ongoing mucosal inflammation with
197 endoscopic signs of disease activity (**Fig. 4i**, grey arrow), despite achieving clinical remission
198 under EEN therapy. Accordingly, FMT 1 from MP3 induced severe inflammation in all recipient
199 *Il10*$^{-/-}$ mice (**Fig. 4j** histopathology score in *Il10*$^{-/-}$ = 7.3 ± 0.8 *vs*. WT = 1.3 ± 0.5, p = 0.0022;
200 **Supplementary Fig. 3c** H&E). In contrast to MP1 and MP2 (**Fig. 4d, e**), EEN-like medium in
201 the chemostat model did not change the inflammatory phenotype in IBD-susceptible mice
202 (MP3-FMT 3, **Fig. 4j** histopathology score in *Il10*$^{-/-}$ = 6.0 ± 1.3 *vs*. WT = 1.6 ± 1.0, p = 0.0006;
203 **Fig. 4k,** H&E, *Tnf* p = 0.0022 for dist. colon and (**Supplementary Fig. 3d**) prox. colon;
204 **Supplementary Fig. 3c**). However, introducing EEN-like diet decreased the level of disease
205 severity after MP3-FMT 4 in most *Il10*$^{-/-}$ mice (**Fig. 4j** histopathology score in EEN-like-fed
206 *Il10*$^{-/-}$ = 3.2 ± 3.1 *vs*. WT = 1.3 ± 0.5, p = n.s.; **Fig. 4k** H&E, *Tnf* p = n.s dist. colon;
207 **Supplementary Fig. 3c, d,** *Tnf* p = 0.0022 for prox. colon) and significantly reduced disease
208 activity compared to the chow-fed group (**Fig. 4j** FMT 3 *vs*. FMT 4**,** histopathology score in
209 EEN-like-fed *Il10*$^{-/-}$ = 3.2 ± 3.1, p = 0.0407 (data not shown); **Fig. 4k** H&E, **Supplementary**
210 **Fig. 3c**). An additional sample of MP2 after clinical relapse was tested under conditions of the
211 extended EEN-like feeding (**Fig. 4c**, grey arrow), and contrary to MP3, the MP2 relapse sample
212 was resistant to EEN induced protection (**Extended Data Fig. 3e-j**). These findings suggest
213 that sustained EEN-like feeding increased the chance to prevent recurrence, but efficacy of
214 repeated EEN decreases with a second course.

215 **Individual strain signatures in gnotobiotic *Il10*$^{-/-}$ mice convey protective function of**
216 **patient's microbiota in response to diet**

217 To investigate bacterial strain profiles responsible for the mouse disease phenotypes (**Fig. 4**),
218 we performed metagenomic analyses of all 54 *Il10*$^{-/-}$ mice from MP1-MP3 (**Fig. 5a-c,** triangles:
219 red - active disease, green - inactive disease; **Extended Data Fig. 4a**). Out of 105 strains
220 detected in MP1, 66 were specific to mice with active disease, while only four were specific to
221 inactive disease (**Fig. 5d,** upper Venn diagram (Vd)). Strains in MP2 mice were skewed
222 towards being specific to inactive disease (**Fig. 5d,** middle Vd), consistent with lower disease
223 activity in MP2 and fewer mice with active disease. Strains in MP3 mice were somewhat less
224 skewed towards being specific to active disease despite a higher number of MP3 mice having
225 active disease (**Fig. 5d,** lower Vd), perhaps because the same microbiota was transferred but
226 only the diet was different between FMT 3 and 4.

227 Motivated by these differences, we next sought to identify species, strains, and metabolites
228 that distinguished active *vs*. inactive *Il10*$^{-/-}$ mice. Dozens of species showed significant
229 differential abundance after the transfer experiments of MP1 (40, **Fig. 5e**), MP2 (17, **Fig. 5f**)
230 and MP3 (12, **Fig. 5g**). *E. clostridioformis, E. bolteae* and *Clostridium innocuum* are the top
231 significant species in inactive mice of the MP1, MP2 and MP3, respectively. *Akkermansia*
232 *muciniphila, Mediterraneibacter gnavus* and *Bacteroides* ssp. were most dominant in mice with
233 active disease (**Fig. 5e**). SPLS-DA of untargeted metabolomics from mouse gut content
234 separated active and inactive mice in the respective transfer experiments independent of
235 dietary exposure (**Fig. 5h-j,** PCA in **Extended Data Fig. 5a-c**). Several bile acids (BA) were
236 highlighted as differentially abundant, which was confirmed in the targeted measurement
237 primary taurine conjugated and secondary unconjugated BA (**Extended Data Fig. 4b, c**).
238 These results clearly demonstrate that despite the model patients having personalized strain
239 composition (**Fig. 6a,** upper left Vd), disease activity in gnotobiotic mice receiving FMTs was
240 consistently associated with a number of metabolic and species-level taxonomic differences.
241 Finally, we investigated the 178 species detected across all transfer experiments, including 22
242 species shared between MP1-MP3 transfer experiments into *Il10*$^{-/-}$ mice (**Fig. 6a,** upper right
243 Vd). In total, 31 species were specific to active disease and five to inactive disease (**Fig. 6a,**
244 lower Vd). Linear discriminant analysis Effect Size (LEfSe) determined 40 species that were
245 differentially abundant between mice with active *vs*. inactive disease, each with individual
246 strain repertoires in samples from the three different MPs (**Fig. 6a, b**). SPLS-DA of the
247 combined untargeted metabolomics dataset confirmed distinct clusters for active and inactive
248 disease independent of MP1-3 donor samples (**Fig. 6c**, **Extended Data Fig. 5d-e**), suggesting
249 that individual strain profiles convey protective or aggressive responses in the IBD susceptible
250 host (**Supplement Fig. 4**). Furthermore, differentially abundant species in humanized mice
251 showed individual patterns associated with EEN and EEN cessation in the CD patient cohort
252 (**Fig. 6d**), underscoring the clinical relevance of the differences we observed in our mouse
253 FMT experiments.

254 Together, these findings demonstrate that individual species and strain signatures prevent or
255 cause IBD-like inflammation in gnotobiotic mice. Most importantly, we provide evidence that
256 EEN therapy creates explicit functional changes of temporally and individually variable
257 microbiome profiles.

258 **Discussion**

259 We followed 78 pediatric IBD patients longitudinally, focusing on 20 newly diagnosed CD
260 patients receiving EEN as first-line treatment. Our results corroborate previous observations
261 that EEN is highly effective at inducing remission. We demonstrate that protective functions of
262 EEN therapy are mediated through diet-induced changes in patient microbiomes despite
263 considerable variations in individual microbiota over time. Dietary exposure of individual
264 patient-derived fecal microbiota in chemostat models and subsequent transfer into IBD-
265 relevant GF mice strongly indicates a causal role of EEN-mediated changes in the microbiome
266 independent of host responses. Notably, we demonstrate that a variety of individually different
267 species and strain signatures convey protective or aggressive disease phenotype in the model
268 systems, confirming the highly personalized strain-level dynamics in patients.

269 Longitudinal sampling revealed an integrated network of taxonomic and metabolomic
270 signatures across pediatric CD patients. In line with previous findings[18], EEN therapy was
271 associated with the genus *Enterocloster* (Lachnospiraceae; former genus *Lachnoclostridium)*.
272 In addition, *E. bolteae* and *E. clostridioformis* were the most abundant species in inactive
273 *Il10*$^{-/-}$ mice. Low levels of *Lachnoclostridium* have been associated with CD[19], supporting a
274 protective function of *Enterocloster* in response to EEN therapy. Nevertheless, taxonomic shifts
275 at the cessation of EEN were highly patient-specific. For example, while in the majority of
276 patients, *E. bolteae* (zOTU5) was at much higher relative abundance during EEN compared to
277 PostEEN, the dominant strains in many patients changed over this transition, and most strains
278 were detected in just one subject. This individual diversity and turnover contribute to challenges
279 in predicting taxonomic responses to dietary changes globally. Antibiotics and pre-existing
280 dysbiosis are both associated with increased strain engraftment in patients receiving fecal
281 microbiota transplants[20]. Likewise, the microbiome perturbation caused by EEN - and its
282 cessation - may encourage strain turnover, with potentially complex consequences for
283 microbial function after therapy.
284 Beyond taxonomic alterations, we identified 10 metabolites associated with EEN treatment and
285 68 metabolites associated with PostEEN samples. Independently, metagenomic analysis
286 highlighted 577 bacterial gene functions with substantial changes in response to EEN,
287 suggesting specific metabolic adaptations of the microbiota to host diets. Modulen IBD® is
288 characterized by easily digestible carbohydrates and high fat content, including medium-chain
289 triglycerides[9]. Our integrated network analysis highlighted caprylic (C8:0), decanoic (C10:0),

290 and lauric (C12:0) acids as associated with protective EEN signatures. These medium-chain
291 fatty acids (MCFAs) are part of the EEN formula and mediate anti-bacterial and anti-
292 inflammatory functions[21–23]. Diets high in fat trigger release of bile acids[24], providing a rationale
293 for *C. innocuum* and *Hungatella hathewayi* to be part of protective EEN signatures[25,26].
294 Concordantly, our untargeted metabolomics analysis identified several BA as differentially
295 abundant, highlighting a potential microbial conversion of primary to secondary bile acids in
296 non-inflamed *Il10*$^{-/-}$ mice, potentially promoting wound healing and epithelial regeneration[24]. In
297 a recent study (FARMM), EEN specifically affected amino acid pathways in the microbiome
298 creating a metabolite milieu low in bacteria-derived indoles[27], which was also low abundant in
299 the EEN-like mouse diet. In addition, EEN-related protective effects in *Il10*$^{-/-}$ mice are partially
300 mediated by isobutyrate production[28], supporting the hypothesis that microbiota and metabolite
301 changes contribute to the EEN therapeutic efficacy.

302 In healthy humans, dietary fiber intake supports beneficial functions of the gastrointestinal
303 tract[29]. In animal models, low fiber diets induce adverse microbiota changes associated with
304 impaired intestinal barrier integrity and bacteria-related mucus degradation[30,31], highlighting
305 the fiber paradox in understanding EEN-mediated anti-inflammatory mechanisms in IBD.
306 Dietary fiber consists of complex carbohydrates, which are resistant to digestion and
307 absorption by the host. However, dietary fiber degradation and availability for the host depends
308 on the fermenting potential of host-specific microbial communities, which are modified by
309 intestinal inflammation[29,32,33]. Using the combined gut chemostat-to-mouse transfer approach,
310 we showed that a fiber-free EEN-like medium maintains the anti-inflammatory and remitting
311 phenotype associated with EEN therapy. Concordantly, the protective effect of EEN-
312 conditioned microbiota is reversible upon exposure to fiber-repleted diet and potentially
313 resistant to repetitive EEN as shown before[12]. Recent studies have demonstrated that fiber-
314 free diets prevent and diminish the colonization of identified pathobionts in different CD-like
315 mouse models[34,35], supporting our hypothesis that EEN therapy directly creates protective
316 niches in the gut microbiome. Preserving beneficial microbiome signatures after cessation of
317 EEN may be a new approach to guide mucosal healing and remission in pediatric CD[36]. In our
318 IBD cohort, 40% (8/20) of pediatric CD patients relapsed within the first year after EEN
319 treatment, highlighting the necessity to maintain remitting conditions. Our data clearly
320 demonstrate that EEN therapy mediates protective changes in individually variant microbiome
321 profiles, leading towards personalized patient-to-patient species and strain signatures. These
322 findings support the idea to develop patient-tailored maintenance strategies in pediatric CD
323 involving combinations of personalized nutritional and bacterial interventions.

324

325

Funding

Funded by the Deutsche Forschungsgemeinschaft (DFG, German Research Foundation) – project number 395357507 (SFB 1371, Microbiome Signatures) and The Leona M. and Harry B. Helmsley Charitable Trust (project numbers 2847 and 2304-05970). TS is supported by the Medical & Clinician Scientist Program (MCSP) of the Faculty of Medicine at LMU Munich. Salary for DHäcker was supported by the National Research Foundation, Prime Minister's Office, Singapore under its Campus for Research Excellence and Technological Enterprise (CREATE) programe.

Conflict of interest

DHaller served on the Microbiome Expert Panel from Reckitt Benckiser Health Limited. TS received lecture honoraria from Nutricia and MSD and travel support from Abbvie and Ferring outside the submitted work.

Acknowledgement

We thank the patients and their families for participating in our research.

Author contribution

DHaller and TS are responsible for the conceptual design of the study; DHäcker and DHaller designed the *ex vivo* experiments; KSiebert, HHölz, JHeetmeyer, FDeZen, GLeThi, TS: collected and prepared clinical data and samples, accompanied, followed and characterized patients, analysis of clinical data; HHölz, TS recruited patients; DHäcker, HHeimes, AMetwaly and DHaller performed and interpreted mouse and fermenter experiments; DHäcker performed 16S rRNA gene amplicon and corresponding statistical analysis; CM, QM, KSocas, ML, KK performed metabolomics with statistical analysis; KSiebert, DHäcker, NK, AMetwaly, ML responsible for integration of clinical metadata with 16S and metabolomics as well as sample selection and performance of data integration and network analysis; NK, ML, PJK performed 16S & untargeted metabolomics data integration, untargeted metabolomics data analyses; BS, AMahapatra, KSP performed metagenomic sequencing and analyses; KN provided 16S rRNA gene amplicon and metagenome sequencing and support for analysis; DHäcker, KSiebert, BS, NK, KSP, TS and DHaller evaluated and interpreted data and wrote the manuscript; All authors provided input on the manuscript, critically revised and approved the final version of the manuscript.

ORCID IDs

Deborah Häcker https://orcid.org/0000-0001-7914-9470
Kolja Siebert https://orcid.org/0009-0005-8083-7074
Byron J Smith https://orcid.org/0000-0002-0182-404X
Nikolai Köhler https://orcid.org/0000-0002-5103-883X
Aritra Mahapatra https://orcid.org/0000-0003-0078-8590
Amira Metwaly https://orcid.org/0000-0001-5740-0230
Hannes Hoelz https://orcid.org/0000-0002-7208-6195
Quirin Manz https://orcid.org/0000-0002-5706-2718
Jeannine Heetmeyer https://orcid.org/0000-0002-0599-9613
Katharina Socas https://orcid.org/0009-0003-8625-4879
Giang Le Thi https://orcid.org/0000-0002-2504-9551
Chen Meng https://orcid.org/0000-0002-5968-6719
Karin Kleigrewe https://orcid.org/0000-0002-7718-0252
Klaus Neuhaus https://orcid.org/0000-0002-6020-2814
Markus List https://orcid.org/0000-0002-0941-4168
Katherine S Pollard https://orcid.org/0000-0002-9870-6196
Tobias Schwerd https://orcid.org/0000-0002-2281-4852
Dirk Haller http://orcid.org/0000-0002-6977-4085

377 **References**

378 1. Torres, J., Mehandru, S., Colombel, J. F. & Peyrin-Biroulet, L. Crohn's disease. *Lancet*
379 **389**, 1741–1755 (2017).

380 2. Kuenzig, M. E. *et al.* Twenty-first Century Trends in the Global Epidemiology of
381 Pediatric-Onset Inflammatory Bowel Disease: Systematic Review. *Gastroenterology*
382 **162**, 1147-1159.e4 (2022).

383 3. Kaplan, G. G. & Ng, S. C. Understanding and Preventing the Global Increase of
384 Inflammatory Bowel Disease. *Gastroenterology* **152**, 313-321.e2 (2017).

385 4. Liu, Z. *et al.* Genetic architecture of the inflammatory bowel diseases across East Asian
386 and European ancestries. *Nat Genet* **55**, 796 (2023).

387 5. Renz, H. *et al.* Gene-environment interactions in chronic inflammatory disease. *Nature*
388 *Immunology 2011 12:4* **12**, 273–277 (2011).

389 6. Van Rheenen, P. F. *et al.* The Medical Management of Paediatric Crohn's Disease: an
390 ECCO-ESPGHAN Guideline Update. *J Crohns Colitis* **15**, 171–194 (2020).

391 7. Agrawal, M., Spencer, E. A., Colombel, J. F. & Ungaro, R. C. Approach to the
392 Management of Recently Diagnosed Inflammatory Bowel Disease Patients: A User's
393 Guide for Adult and Pediatric Gastroenterologists. *Gastroenterology* **161**, 47–65 (2021).

394 8. Bischoff, S. C. *et al.* ESPEN guideline on Clinical Nutrition in inflammatory bowel
395 disease. *Clin Nutr* **42**, 352–379 (2023).

396 9. Logan, M. *et al.* Analysis of 61 exclusive enteral nutrition formulas used in
397 the management of active Crohn's disease—new insights into dietary disease triggers.
398 *Aliment Pharmacol Ther* **51**, 935–947 (2020).

399 10. Logan, M. *et al.* The reduction of faecal calprotectin during exclusive enteral nutrition is
400 lost rapidly after food re-introduction. *Aliment Pharmacol Ther* **50**, 664 (2019).

401 11. Schwerd, T. *et al.* Exclusive enteral nutrition in active pediatric Crohn disease: Effects
402 on intestinal microbiota and immune regulation. *Journal of Allergy and Clinical*
403 *Immunology* **138**, 592–596 (2016).

404 12. Frivolt, K. *et al.* Repeated exclusive enteral nutrition in the treatment of paediatric
405 Crohn's disease: Predictors of efficacy and outcome. *Aliment Pharmacol Ther* **39**, 1398–
406 1407 (2014).

13. Metwaly, A., Reitmeier, S. & Haller, D. Microbiome risk profiles as biomarkers for inflammatory and metabolic disorders. *Nature Reviews Gastroenterology & Hepatology 2022 19:6* **19**, 383–397 (2022).

14. Schirmer, M., Garner, A., Vlamakis, H. & Xavier, R. J. Microbial genes and pathways in inflammatory bowel disease. *Nat Rev Microbiol* **17**, 497 (2019).

15. Lavelle, A. & Sokol, H. Gut microbiota-derived metabolites as key actors in inflammatory bowel disease. *Nature Reviews Gastroenterology & Hepatology 2020 17:4* **17**, 223–237 (2020).

16. Smith, B. J., Li, X., Shi, Z. J., Abate, A. & Pollard, K. S. Scalable Microbial Strain Inference in Metagenomic Data Using StrainFacts. *Frontiers in Bioinformatics* **2**, (2022).

17. Metwaly, A. *et al.* Integrated microbiota and metabolite profiles link Crohn's disease to sulfur metabolism. *Nature Communications 2020 11:1* **11**, 1–15 (2020).

18. Jiang, J., Chen, L., Chen, Y. & Chen, H. Exclusive enteral nutrition remodels the intestinal flora in patients with active Crohn's disease. *BMC Gastroenterol* **22**, (2022).

19. Vich Vila, A. *et al.* Gut microbiota composition and functional changes in inflammatory bowel disease and irritable bowel syndrome. *Sci Transl Med* **10**, (2018).

20. Podlesny, D. *et al.* Identification of clinical and ecological determinants of strain engraftment after fecal microbiota transplantation using metagenomics. *Cell Rep Med* **3**, 100711 (2022).

21. Yang, H. T. *et al.* Lauric acid is an inhibitor of Clostridium difficile growth in vitro and reduces inflammation in a mouse infection model. *Front Microbiol* **8**, 2635 (2018).

22. Kabara, J. J., Swieczkowski, D. M., Conley, A. J. & Truant, J. P. Fatty acids and derivatives as antimicrobial agents. *Antimicrob Agents Chemother* **2**, 23–28 (1972).

23. Huang, W. C. *et al.* Anti-bacterial and anti-inflammatory properties of capric acid against Propionibacterium acnes: A comparative study with lauric acid. *J Dermatol Sci* **73**, 232–240 (2014).

24. Sorrentino, G. *et al.* Bile Acids Signal via TGR5 to Activate Intestinal Stem Cells and Epithelial Regeneration. *Gastroenterology* **159**, 956-968.e8 (2020).

25. Xiao, F. *et al.* Exclusive Enteral Nutrition Exerts Anti-Inflammatory Effects through Modulating Microbiota, Bile Acid Metabolism, and Immune Activities. *Nutrients* **14**, 4463 (2022).

438 26. Lv, Y. *et al.* The impact of exclusive enteral nutrition on the gut microbiome and bile acid
439 metabolism in pediatric Crohn's disease. *Clinical Nutrition* **42**, 116–128 (2023).

440 27. Tanes, C. *et al.* Role of dietary fiber in the recovery of the human gut microbiome and
441 its metabolome. *Cell Host Microbe* **29**, 394-407.e5 (2021).

442 28. Pereira, G. V. *et al.* Unravelling specific diet and gut microbial contributions to
443 inflammatory bowel disease. *bioRxiv* 2022.04.03.486886 (2022)
444 doi:10.1101/2022.04.03.486886.

445 29. Gill, S. K., Rossi, M., Bajka, B. & Whelan, K. Dietary fibre in gastrointestinal health and
446 disease. *Nature Reviews Gastroenterology & Hepatology 2020 18:2* **18**, 101–116
447 (2020).

448 30. Schroeder, B. O. *et al.* Bifidobacteria or Fiber Protects against Diet-Induced Microbiota-
449 Mediated Colonic Mucus Deterioration. *Cell Host Microbe* **23**, 27-40.e7 (2018).

450 31. Desai, M. S. *et al.* A Dietary Fiber-Deprived Gut Microbiota Degrades the Colonic Mucus
451 Barrier and Enhances Pathogen Susceptibility. *Cell* **167**, 1339-1353.e21 (2016).

452 32. Haskey, N., Gold, S. L., Faith, J. J. & Raman, M. To Fiber or Not to Fiber: The Swinging
453 Pendulum of Fiber Supplementation in Patients with Inflammatory Bowel Disease.
454 *Nutrients 2023, Vol. 15, Page 1080* **15**, 1080 (2023).

455 33. Armstrong, H., Mander, I., Zhang, Z., Armstrong, D. & Wine, E. Not All Fibers Are Born
456 Equal; Variable Response to Dietary Fiber Subtypes in IBD. *Front Pediatr* **8**, 620189
457 (2021).

458 34. Kuffa, P. *et al.* Fiber-deficient diet inhibits colitis through the regulation of the niche and
459 metabolism of a gut pathobiont. *Cell Host Microbe* (2023)
460 doi:10.1016/J.CHOM.2023.10.016.

461 35. Metwaly, A. *et al.* Diet prevents the expansion of segmented filamentous bacteria and
462 ileo-colonic inflammation in a model of Crohn's disease. *Microbiome* **11**, 66 (2023).

463 36. Turner, D. *et al.* STRIDE-II: An Update on the Selecting Therapeutic Targets in
464 Inflammatory Bowel Disease (STRIDE) Initiative of the International Organization for the
465 Study of IBD (IOIBD): Determining Therapeutic Goals for Treat-to-Target strategies in
466 IBD. *Gastroenterology* **160**, 1570–1583 (2021).

467 37. Levine, A. *et al.* ESPGHAN Revised Porto Criteria for the Diagnosis of Inflammatory
468 Bowel Disease in Children and Adolescents. *J Pediatr Gastroenterol Nutr* **58**, 795–806
469 (2014).

470 38. Turner, D. *et al.* Management of paediatric ulcerative colitis, part 1: Ambulatory Care-An
471 Evidence-based Guideline From European Crohn's and Colitis Organization and
472 European Society of Paediatric Gastroenterology, Hepatology and Nutrition. *J Pediatr*
473 *Gastroenterol Nutr* **67**, 257–291 (2018).

474 39. Turner, D. *et al.* Management of paediatric ulcerative colitis, part 2: Acute severe colitis
475 - An evidence-based consensus guideline from the european Crohn's and colitis
476 organization and the european society of paediatric gastroenterology, hepatology and
477 nutrition. *J Pediatr Gastroenterol Nutr* **67**, 292–310 (2018).

478 40. Schult, D. *et al.* Gut bacterial dysbiosis and instability is associated with the onset of
479 complications and mortality in COVID-19. *Gut Microbes* **14**, (2022).

480 41. Livak, K. J. & Schmittgen, T. D. Analysis of Relative Gene Expression Data Using Real-
481 Time Quantitative PCR and the 2−ΔΔCT Method. *Methods* **25**, 402–408 (2001).

482 42. Püngel, D. *et al.* Bifidobacterium breve UCC2003 Exopolysaccharide Modulates the
483 Early Life Microbiota by Acting as a Potential Dietary Substrate. *Nutrients* **12**, 948
484 (2020).

485 43. Macfarlane, G. T., Macfarlane, S. & Gibson, G. R. Validation of a three-stage compound
486 continuous culture system for investigating the effect of retention time on the ecology
487 and metabolism of bacteria in the human colon. *Microb Ecol* **35**, 180–187 (1998).

488 44. Gibson, G. R. & Wang, X. Enrichment of bifidobacteria from human gut contents by
489 oligofructose using continuous culture. *FEMS Microbiol Lett* **118**, 121–127 (1994).

490 45. Cinquin, C., Le Blay, G., Fliss, I. & Lacroix, C. Immobilization of infant fecal microbiota
491 and utilization in an in vitro colonic fermentation model. *Microb Ecol* **48**, 128–138 (2004).

492 46. Poeker, S. A. *et al.* Stepwise Development of an in vitro Continuous Fermentation Model
493 for the Murine Caecal Microbiota. *Front Microbiol* **10**, (2019).

494 47. Reitmeier, S., Kiessling, S., Neuhaus, K. & Haller, D. Comparing Circadian Rhythmicity
495 in the Human Gut Microbiome. *STAR Protoc* **1**, 100148 (2020).

496 48. Lagkouvardos, I., Fischer, S., Kumar, N. & Clavel, T. Rhea: A transparent and modular
497 R pipeline for microbial profiling based on 16S rRNA gene amplicons. *PeerJ* **2017**,
498 (2017).

499 49. Chen, J. *et al.* Associating microbiome composition with environmental covariates using
500 generalized UniFrac distances. *Bioinformatics* **28**, 2106–2113 (2012).

501 50. Jost, L. Partitioning diversity into independent alpha and beta components. *Ecology* **88**,
502 2427–2439 (2007).

503 51. Subramanian, B., Gao, S., Lercher, M. J., Hu, S. & Chen, W. H. Evolview v3: a
504 webserver for visualization, annotation, and management of phylogenetic trees. *Nucleic*
505 *Acids Res* **47**, W270–W275 (2019).

506 52. Segata, N. *et al.* Metagenomic biomarker discovery and explanation. *Genome Biol* **12**,
507 R60 (2011).

508 53. Bolger, A. M., Lohse, M. & Usadel, B. Trimmomatic: a flexible trimmer for Illumina
509 sequence data. *Bioinformatics* **30**, 2114–2120 (2014).

510 54. Langmead, B. & Salzberg, S. L. Fast gapped-read alignment with Bowtie 2. *Nature*
511 *Methods 2012 9:4* **9**, 357–359 (2012).

512 55. Shi, Z. J., Dimitrov, B., Zhao, C., Nayfach, S. & Pollard, K. S. Fast and accurate
513 metagenotyping of the human gut microbiome with GT-Pro. *Nature Biotechnology 2021*
514 *40:4* **40**, 507–516 (2021).

515 56. Almeida, A. *et al.* A unified catalog of 204,938 reference genomes from the human gut
516 microbiome. *Nature Biotechnology 2020 39:1* **39**, 105–114 (2020).

517 57. Zhao, C., Dimitrov, B., Goldman, M., Nayfach, S. & Pollard, K. S. MIDAS2: Metagenomic
518 Intra-species Diversity Analysis System. *Bioinformatics* **39**, (2023).

519 58. Reiter, S. *et al.* Development of a Highly Sensitive Ultra-High-Performance Liquid
520 Chromatography Coupled to Electrospray Ionization Tandem Mass Spectrometry
521 Quantitation Method for Fecal Bile Acids and Application on Crohn's Disease Studies. *J*
522 *Agric Food Chem* **69**, 5238–5251 (2021).

523 59. Kessner, D., Chambers, M., Burke, R., Agus, D. & Mallick, P. ProteoWizard: open source
524 software for rapid proteomics tools development. *Bioinformatics* **24**, 2534–2536 (2008).

525 60. Smith, C. A., Want, E. J., O'Maille, G., Abagyan, R. & Siuzdak, G. XCMS: processing
526 mass spectrometry data for metabolite profiling using nonlinear peak alignment,
527 matching, and identification. *Anal Chem* **78**, 779–787 (2006).

528 61. Wishart, D. S. *et al.* HMDB 4.0: the human metabolome database for 2018. *Nucleic*
529 *Acids Res* **46**, D608–D617 (2018).

530 62. Tsugawa, H. *et al.* MS-DIAL: data-independent MS/MS deconvolution for
531 comprehensive metabolome analysis. *Nature Methods 2015 12:6* **12**, 523–526 (2015).

63. Dührkop, K. *et al.* SIRIUS 4: a rapid tool for turning tandem mass spectra into metabolite structure information. *Nature Methods 2019 16:4* **16**, 299–302 (2019).

64. Singh, A. *et al.* DIABLO: an integrative approach for identifying key molecular drivers from multi-omics assays. *Bioinformatics* **35**, 3055–3062 (2019).

65. Benjamini, Y. & Hochberg, Y. Controlling the False Discovery Rate: A Practical and Powerful Approach to Multiple Testing. *Journal of the Royal Statistical Society: Series B (Methodological)* **57**, 289–300 (1995).

66. Blondel, V. D., Guillaume, J. L., Lambiotte, R. & Lefebvre, E. Fast unfolding of communities in large networks. *Journal of Statistical Mechanics: Theory and Experiment* **2008**, P10008 (2008).

67. Csárdi, G. & Nepusz, T. The igraph software package for complex network research. *InterJournal, Complex Systems* **5**, 1–9 (2006).

68. Hagberg, A. A., Lanlgov -Los, Schult, D. A. & Swart, P. J. S. Exploring Network Structure, Dynamics, and Function using NetworkX. (2008).

69. Yoon, S. H. *et al.* Introducing EzBioCloud: A taxonomically united database of 16S rRNA gene sequences and whole-genome assemblies. *Int J Syst Evol Microbiol* **67**, 1613–1617 (2017).

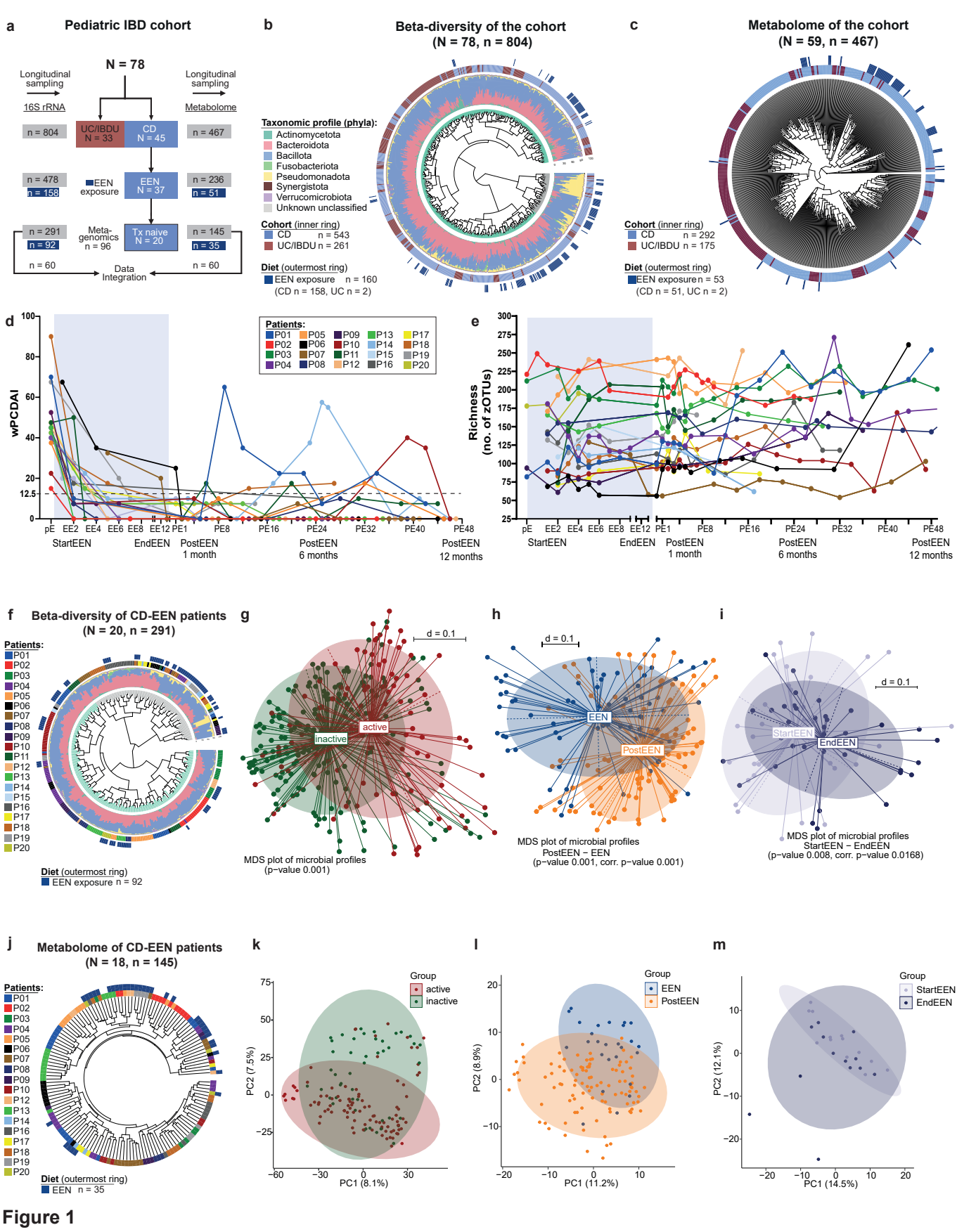
a
Pediatric IBD cohort
N = 78
Longitudinal sampling
16S rRNA
Longitudinal sampling
Metabolome
n = 804
UC/IBDU N = 33
CD N = 45
n = 467
n = 478
n = 158
EEN exposure
EEN N = 37
n = 236
n = 51
n = 291
n = 92
Meta-genomics n = 96
Tx naive N = 20
n = 145
n = 35
n = 60
Data Integration
n = 60
b
Beta-diversity of the cohort
(N = 78, n = 804)
Taxonomic profile (phyla):
Actinomycetota
Bacteroidota
Bacillota
Fusobacteriota
Pseudomonadota
Synergistota
Verrucomicrobiota
Unknown unclassified
Cohort (inner ring)
CD n = 543
UC/IBDU n = 261
Diet (outermost ring)
EEN exposure n = 160
(CD n = 158, UC n = 2)
c
Metabolome of the cohort
(N = 59, n = 467)
Cohort (inner ring)
CD n = 292
UC/IBDU n = 175
Diet (outermost ring)
EEN exposure n = 53
(CD n = 51, UC n = 2)
d
wPCDAI
Patients:
P01 P02 P03 P04 P05 P06 P07 P08 P09 P10 P11 P12 P13 P14 P15 P16 P17 P18 P19 P20
pE EE2 EE4 EE6 EE8 EE12 PE1 PE8 PE16 PE24 PE32 PE40 PE48
StartEEN
EndEEN
PostEEN 1 month
PostEEN 6 months
PostEEN 12 months
e
Richness (no. of zOTUs)
pE EE2 EE4 EE6 EE8 EE12 PE1 PE8 PE16 PE24 PE32 PE40 PE48
StartEEN
EndEEN
PostEEN 1 month
PostEEN 6 months
PostEEN 12 months
f
Beta-diversity of CD-EEN patients
(N = 20, n = 291)
Patients:
P01 P02 P03 P04 P05 P06 P07 P08 P09 P10 P11 P12 P13 P14 P15 P16 P17 P18 P19 P20
Diet (outermost ring)
EEN exposure n = 92
g
d = 0.1
active
inactive
MDS plot of microbial profiles
(p−value 0.001)
h
d = 0.1
EEN
PostEEN
MDS plot of microbial profiles
PostEEN − EEN
(p−value 0.001, corr. p−value 0.001)
i
d = 0.1
StartEEN
EndEEN
MDS plot of microbial profiles
StartEEN − EndEEN
(p−value 0.008, corr. p−value 0.0168)
j
Metabolome of CD-EEN patients
(N = 18, n = 145)
Patients:
P01 P02 P03 P04 P05 P06 P07 P08 P09 P10 P12 P13 P14 P16 P17 P18 P19 P20
Diet (outermost ring)
EEN n = 35
k
Group
active
inactive
PC2 (7.5%)
PC1 (8.1%)
l
Group
EEN
PostEEN
PC2 (8.9%)
PC1 (11.2%)
m
Group
StartEEN
EndEEN
PC2 (12.1%)
PC1 (14.5%)

Figure 1

550 ***Fig. 1: Fecal microbial and metabolic changes in response to EEN.***
551 ***a*** *Patients of the Pediatric IBD cohort and longitudinal sampling of 804 and 467 stool samples for 16S rRNA*
552 *amplicon sequencing and metabolome analysis, respectively. Of the 45 CD patients, 37 received Exclusive Enteral*
553 *Nutrition (EEN). Among these 37 patients, 20 were newly diagnosed and treatment (Tx) naïve. Number of CD*
554 *samples that were taken under EEN therapy are highlighted in blue.* ***b*** *Beta-diversity analysis of the fecal microbiota*
555 *in IBD patients. The circular dendrogram shows differences in beta-diversity from the longitudinal microbial profiling*
556 *based on generalized UniFrac distances between 804 samples of 78 patients of the cohort. Taxonomic composition*
557 *of fecal samples at the phylum level is shown as color-coded stacked bar blots around the dendrogram. Bars in the*
558 *first outer ring of the figure show disease phenotypes (CD, UC/IBDU) and EEN treatment in the second outer ring.*
559 ***c*** *Complete clustering of untargeted metabolomic samples with Euclidean distance for 467 longitudinal fecal*
560 *samples from 59 IBD patients, visualized in a circular tree.* ***d – i*** *Visualizations of beta-diversities concerning*
561 *samples from the 20 newly diagnosed pCD patients receiving EEN therapy.* ***c*** *Weighted pediatric Crohn's Disease*
562 *activity index (wPCDAI) over time (EEN shaded blue), remission achieved below 12.5 points (dashed line). pE =*
563 *PreEEN, EE = EEN, PE = PostEEN.* ***e*** *Alpha-diversity plotted as richness (number of zOTUs) over time as in D.* ***f***
564 *Beta-diversity analysis of the fecal microbiota samples. The circular dendrogram shows differences in beta-*
565 *diversities from the longitudinal microbial profiling based on generalized UniFrac distances between the 291 stool*
566 *samples of the 20 patients. Indicated in color code are the patients and samples collected during EEN. Color code*
567 *of taxonomic composition at phylum level as in B.* ***g – i*** *Beta-diversity MDS plots:* ***g*** *Active vs. inactive samples (n*
568 *= 281),* ***h*** *Samples during EEN (at least two weeks on EEN, n = 73) vs. PostEEN (two weeks after end of EEN-*
569 *induced remission, n = 101),* ***i*** *Start of EEN (StartEEN, n = 34)* vs. *the very last matching samples under EEN (week*
570 *6-9, depending on the individual therapy of patients; EndEEN, n = 36).* ***j – m:*** *Visualization of untargeted*
571 *metabolome samples from 18 newly diagnosed pediatric CD patients receiving EEN therapy:* ***j*** *Complete clustering*
572 *with Euclidean distance of longitudinal samples from 18 CD-EEN patients (n = 145),* ***k – m*** *Analyses of untargeted*
573 *metabolomics with representative PCA plots comparing different groups (color codes as indicated). Axes indicate*
574 *principal components (PC), with PC1 representing the most variation (%) and PC2 representing the second most*
575 *variation (%).* ***k*** *Samples during active (n = 99)* vs. *inactive (n = 46) disease.* ***m*** *Samples during EEN (n = 26) and*
576 *PostEEN (n = 100; same cut off as in H),* ***m*** *Start (n = 13)* vs. *end of EEN (n = 13).*

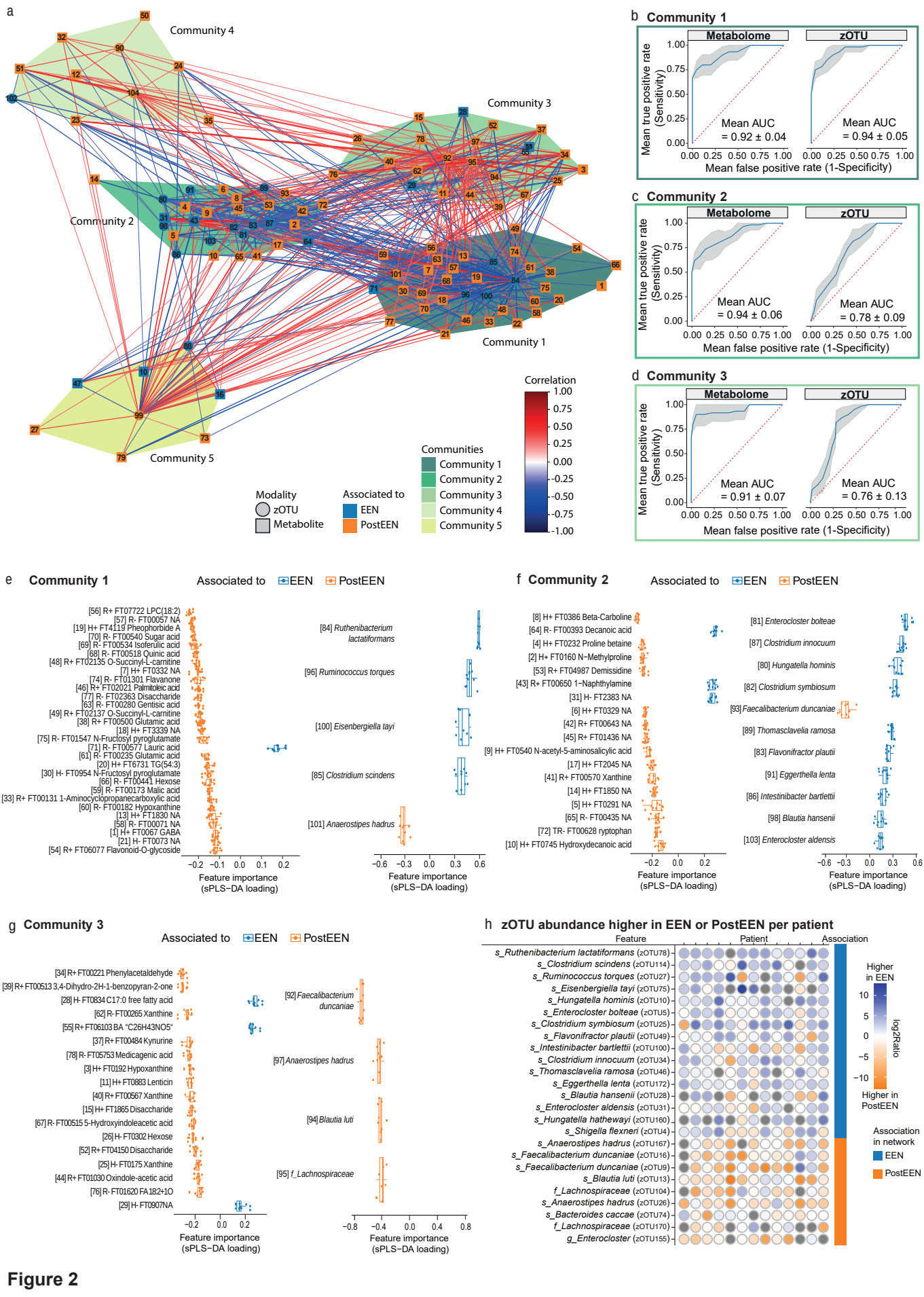
a
Community 1
Community 2
Community 3
Community 4
Community 5
Modality
zOTU
Metabolite
Associated to
EEN
PostEEN
Communities
Correlation
b Community 1
Metabolome
zOTU
Mean true positive rate (Sensitivity)
Mean false positive rate (1-Specificity)
Mean AUC = 0.92 ± 0.04
Mean AUC = 0.94 ± 0.05
c Community 2
Mean AUC = 0.94 ± 0.06
Mean AUC = 0.78 ± 0.09
d Community 3
Mean AUC = 0.91 ± 0.07
Mean AUC = 0.76 ± 0.13
e Community 1
Feature importance (sPLS−DA loading)
[84] Ruthenibacterium lactatiformans
[96] Ruminococcus torques
[100] Eisenbergiella tayi
[85] Clostridium scindens
[101] Anaerostipes hadrus
f Community 2
[81] Enterocloster bolteae
[87] Clostridium innocuum
[80] Hungatella hominis
[82] Clostridium symbiosum
[93] Faecalibacterium duncaniae
[89] Thomasclavelia ramosa
[83] Flavonifractor plautii
[91] Eggerthella lenta
[86] Intestinibacter bartlettii
[98] Blautia hansenii
[103] Enterocloster aldensis
g Community 3
[92] Faecalibacterium duncaniae
[97] Anaerostipes hadrus
[94] Blautia luti
[95] f_Lachnospiraceae
h zOTU abundance higher in EEN or PostEEN per patient
Feature
Patient
Association
Higher in EEN
Higher in PostEEN
log2Ratio
Association in network
EEN
PostEEN

Figure 2

***Fig. 2: Data integration and identification of features for EEN**:*

***a** Correlation network built from selected features based on sPLS-DA-based data integration. Five communities were identified (color coded as indicated). Indicated are zOTUs (circles) and metabolites (squares), their associations to EEN (blue) or PostEEN (orange), and correlation values (lines between features, blue to red). **b - d** ROC curves for metabolome and zOTU features, respectively, for Community 1, 2, and 3, grey area ±1 SD. **e - g** Most important features (i.e., metabolites and zOTUs) for each community with their feature importance for PostEEN (<0, orange) and EEN (>0, blue). One dot represents the loading of the respective feature for a single iteration of the cross-validation procedure (i.e. each iteration is trained on a (stratified) random subset of all data points). **h** Dotplot of patient-specific expression levels of EEN and PostEEN zOTU signatures (N = 13; all of which EEN and PostEEN samples were available) showing individual log fold-changes between expression levels of EEN and PostEEN samples. The mean of expression was used when more than one sample was available per patient and condition, i.e. EEN or PostEEN. Blue, higher expression in EEN samples; orange, higher expression levels in PostEEN samples; white, balanced between conditions; grey, zOTU was not present in the EEN and PostEEN sample. zOTUs identified with SILVA in the network analyses were re-checked using the 16S-based ID tool of EzBioCloud[69] using the database update 2023.08.23, reflecting all taxa published and accepted by IJSEM until April 2023.*

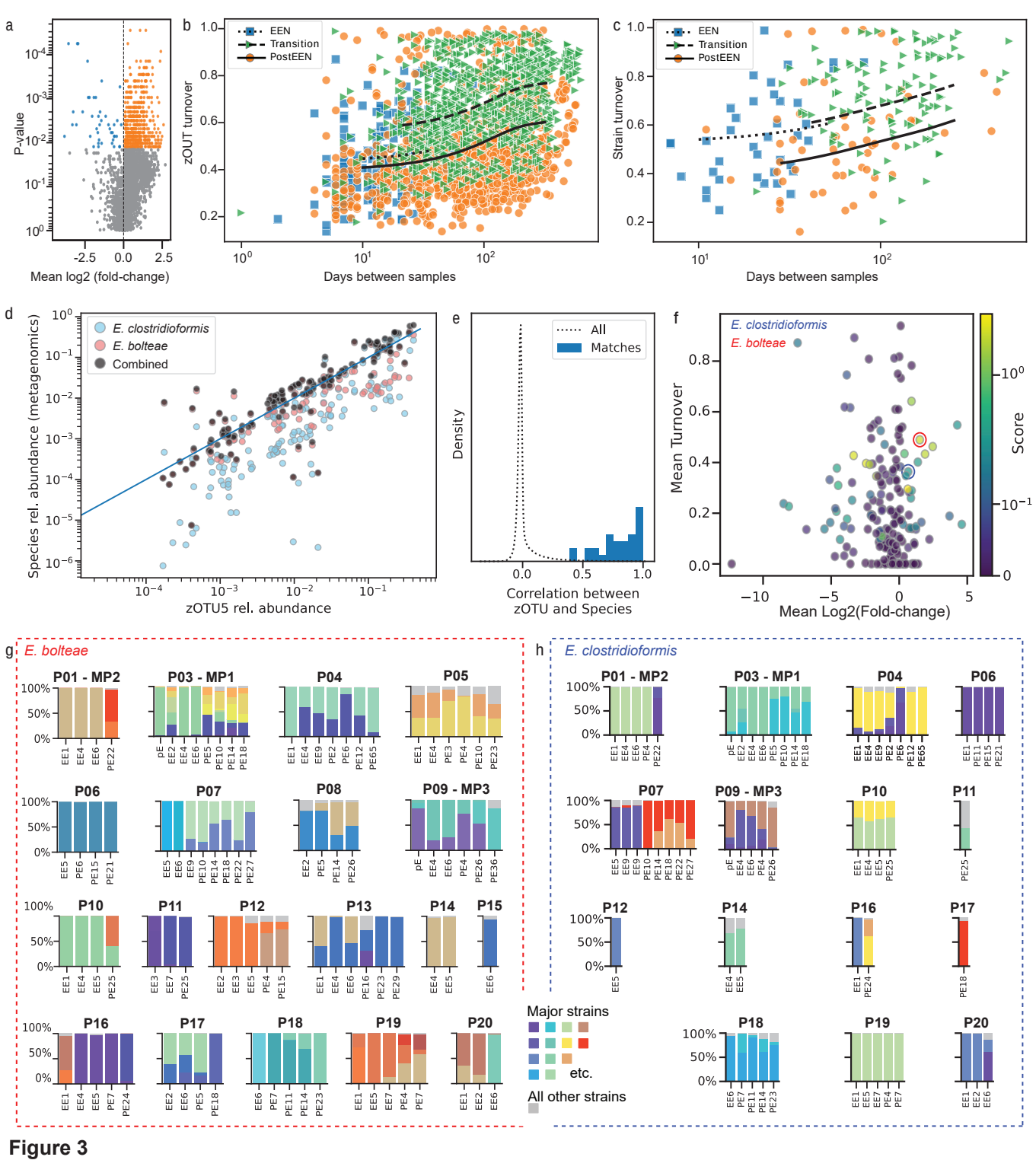
a
P-value
Mean log2 (fold-change)
b
EEN
Transition
PostEEN
zOUT turnover
Days between samples
c
EEN
Transition
PostEEN
Strain turnover
Days between samples
d
E. clostridioformis
E. bolteae
Combined
Species rel. abundance (metagenomics)
zOTU5 rel. abundance
e
All
Matches
Density
Correlation between zOTU and Species
f
E. clostridioformis
E. bolteae
Mean Turnover
Mean Log2(Fold-change)
Score
g
E. bolteae
P01 - MP2
P03 - MP1
P04
P05
P06
P07
P08
P09 - MP3
P10
P11
P12
P13
P14
P15
P16
P17
P18
P19
P20
h
E. clostridioformis
P01 - MP2
P03 - MP1
P04
P06
P07
P09 - MP3
P10
P11
P12
P14
P16
P17
P18
P19
P20
Major strains
etc.
All other strains

Figure 3

Fig. 3 – Species and strain turnover during the transition off of EEN:

a *Volcano plots showing COG functions with significant changes in normalized abundance at the transition off of EEN (Wilcoxon test at false discovery rate (FDR) < 0.1). Here, 45 COGs were at significantly greater relative depth during PostEEN and 532 during EEN.* ***b, c*** *Turnover of taxonomic composition during the transition from EEN to a PostEEN diet of both* ***(b)*** *zOTU and* ***(c)*** *strain compositions. The three lines reflect cubic spline regression of Bray-Curtis dissimilarities against time, averaged across subjects and offset by an independent intercept for each pair type.* ***d*** *Correlation between the relative abundance of zOTU5 and the individual and combined relative abundances of the species* Enterocloster bolteae *and* Enterocloster clostridioformis *determined by quantification with shotgun metagenomes. The blue diagonal represents a 1:1 relationship in relative abundance.* ***e*** *The distribution of correlations between zOTUs and species. In this way, 26 zOTUs matched to one or more metagenomic species (****Extended Data Table 2****), including zOTU5 with each of* E. bolteae *and* E. clostridioformis*, had substantially greater Pearson correlation than unmatched pairs ($p < 10^{-10}$, Mann-Whitney U test).* ***f*** *Characterization of species based on fold-change in relative abundance between EEN and PostEEN samples and average strain-level turnover, defined as the mean Bray-Curtis dissimilarity between within-subject sample pairs. Particularly interesting species were identified based on the product of these two statistics, the number of within-subject sample pairs, and the mean relative abundance (****Extended Data Table 2****). Points are colored based on this score and the two species matched to zOTU5 are circled:* E. bolteae *(red),* E. clostridioformis *(blue). Plots for the 20 highest scoring species are in* ***Supplementary Fig. 2. g, h****. Composition over time of strains within* ***(g)*** E. bolteae *(red box) and* ***(h)*** E. clostridioformis *(blue box), both abundant in the CD-EEN patients: Both species have noteable strain dynamics during and after EEN, but with* E. bolteae *showing higher diversity and turnover. Strain genotypes and fractions were estimated from shotgun metagenomic data. Fractions of abundant strains (colored bars) are shown across samples from individual subjects (P01, P02…), before EEN ("pE" labels on x-axis), during ("EE") and after ("PE"). Strain fractions for the species sum to 1; minor strains are summed together and shown in grey.*

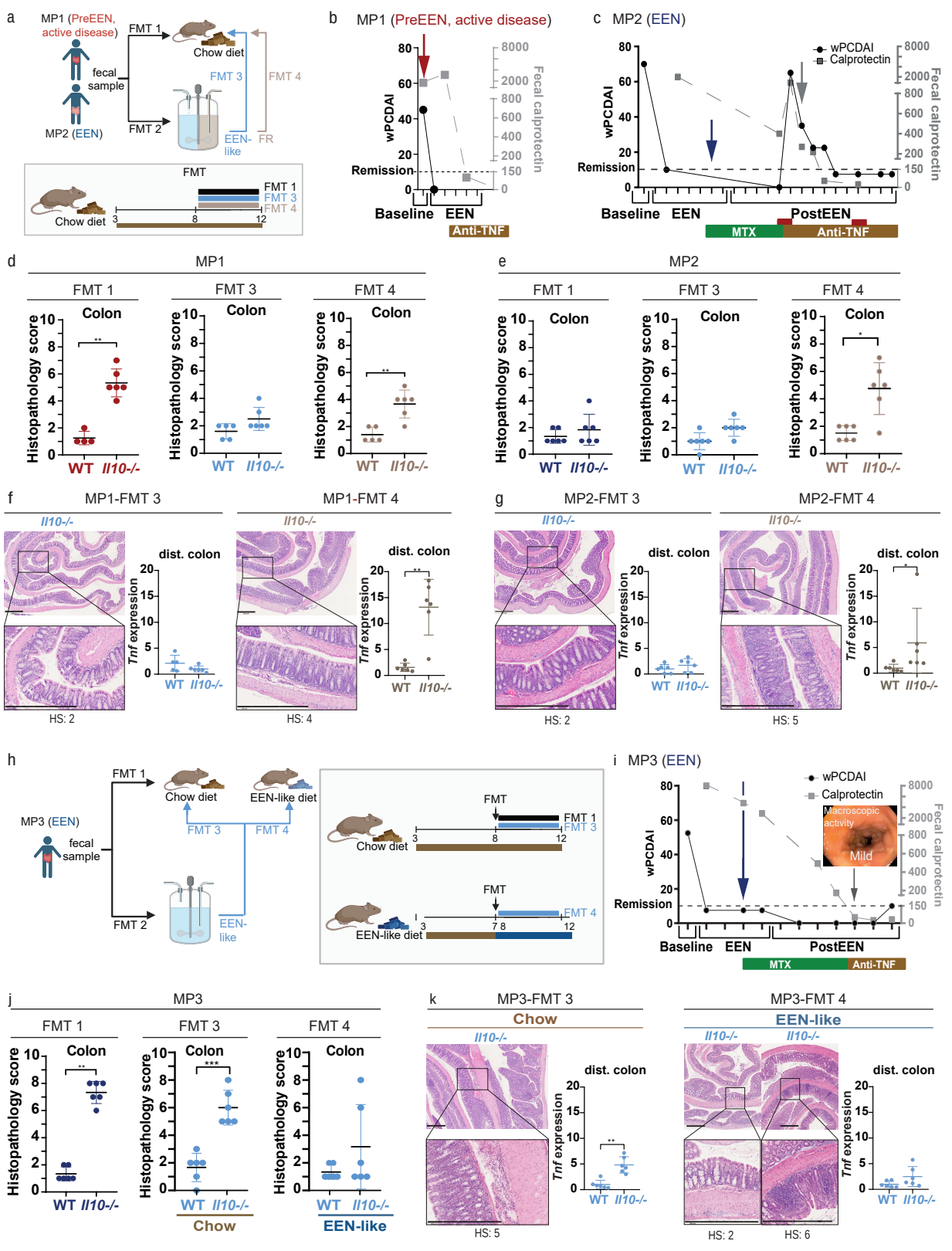
a
MP1 (PreEEN, active disease)
fecal sample
MP2 (EEN)
FMT 1
FMT 2
Chow diet
FMT 3
FMT 4
EEN-like
FR
FMT
Chow diet
b
MP1 (PreEEN, active disease)
wPCDAI
Fecal calprotectin
Remission
Baseline
EEN
Anti-TNF
c
MP2 (EEN)
wPCDAI
Calprotectin
Fecal calprotectin
Remission
Baseline
EEN
PostEEN
MTX
Anti-TNF
d
MP1
FMT 1
FMT 3
FMT 4
Colon
Histopathology score
WT
Il10-/-
e
MP2
f
MP1-FMT 3
MP1-FMT 4
Il10-/-
dist. colon
Tnf expression
HS: 2
HS: 4
g
MP2-FMT 3
MP2-FMT 4
HS: 2
HS: 5
h
MP3 (EEN)
fecal sample
FMT 1
FMT 2
Chow diet
EEN-like diet
FMT 3
FMT 4
EEN-like
FMT
i
MP3 (EEN)
Macroscopic activity
Mild
j
MP3
k
MP3-FMT 3
Chow
MP3-FMT 4
EEN-like
HS: 5
HS: 2
HS: 6

Figure 4

616 ***Fig. 4: Functional validation of gut microbiota-dependent EEN-efficacy using* ex vivo *fermentation and***
617 ***gnotobiotic humanized mice.***

618 ***a*** *Experimental scheme: FMT 1, Patient sample is transferred into GF mice at the age of 8 weeks for 4 weeks.*
619 *Same patient sample is also transferred (FMT 2) in an* ex vivo *gut chemostat model and treated with medium*
620 *simulating EEN (EEN-like, devoid of fibers) or a regular diet (fiber-rich, FR). Fermented sample is transferred (post*
621 ex vivo*) into GF mice (age of 8 weeks) for 4 weeks (FMT 3 - EEN-like medium conditioned, FMT 4 - FR medium*
622 *conditioned).* ***b, c*** *Transfer of patient sample: patients disease state with wPCDAI and fecal calprotectin levels,*
623 *therapy response over time with maintenance therapy (MTX, Anti-TNF) and sampling time point.* ***b*** *Model Patient*
624 *(MP) 1, sample (red arrow) collected PreEEN in active disease.* ***c*** *MP2, sample (blue arrow) collected in EEN*
625 *induced remission.* ***d*** *Mouse histopathology scoring of colon Swiss roles of FMT 1, 3 and 4 from MP1.* ***e*** *Mouse*
626 *histopathology scoring of colon Swiss roles of FMT 1, 3 and 4 from MP2.* ***f, g*** *Mouse transfer experiments from FMT*
627 *3 and 4: Representative (mean of group) H&E stained sections of colonic Swiss roles and corresponding higher*
628 *magnifications for Il10$^{-/-}$ mice (scale bars = 500 µM, HS = histopathology score) respective controls in Extended*
629 *Data Fig 3) with* Tnf *gene expression levels (fold of control) in distal colon.* ***f*** *MP1.* ***g*** *MP2.* ***h*** *Experimental scheme:*
630 *Patient sample from MP3 is transferred into GF mice (FMT 1) at the age of 8 weeks, for 4 weeks. Same patient*
631 *sample is also transferred in an* ex vivo *gut chemostat model and treated with EEN-like medium. Fermented sample*
632 *is transplanted (post* ex vivo*) into GF mice at the age of 8 weeks, for 4 weeks getting either chow diet (FMT 3) or*
633 *EEN-like purified diet (EEN-like) one week prior to FMT (FMT 4).* ***i*** *MP3 sample for transfer (EEN): patients' disease*
634 *state with wPCDAI and fecal calprotectin, therapy response over time, maintenance therapy (MTX, Anti-TNF) and*
635 *sampling time point of transferred fecal sample (blue arrow); grey arrow indicates endoscopy performed in the*
636 *patient PostEEN and the picture taken during endoscopy shows active ileitis.* ***j*** *Mouse histopathology scoring of*
637 *colon Swiss roles of FMT 1, 3 and 4 from MP3.* ***k*** *Mouse transfer experiments from FMT 3 and 4 from MP3:*
638 *Representative (mean of group) H&E stained sections of colonic Swiss roles and corresponding higher*
639 *magnifications for Il10$^{-/-}$ mice (scale bars = 500 µM, HS = histopathology score) respective controls in Extended*
640 *Data Fig 3) with* Tnf *gene expression levels (fold of control) in distal colon.* ***a, h*** *Created with BioRender.com. Data*
641 *are represented by (****d, e, f, g, j, k****) mean ± SD of six biological replicates. P values were calculated by Mann-*
642 *Whitney test. *p < 0.05, **p < 0.01, ***p < 0.001, ****p < 0.0001*

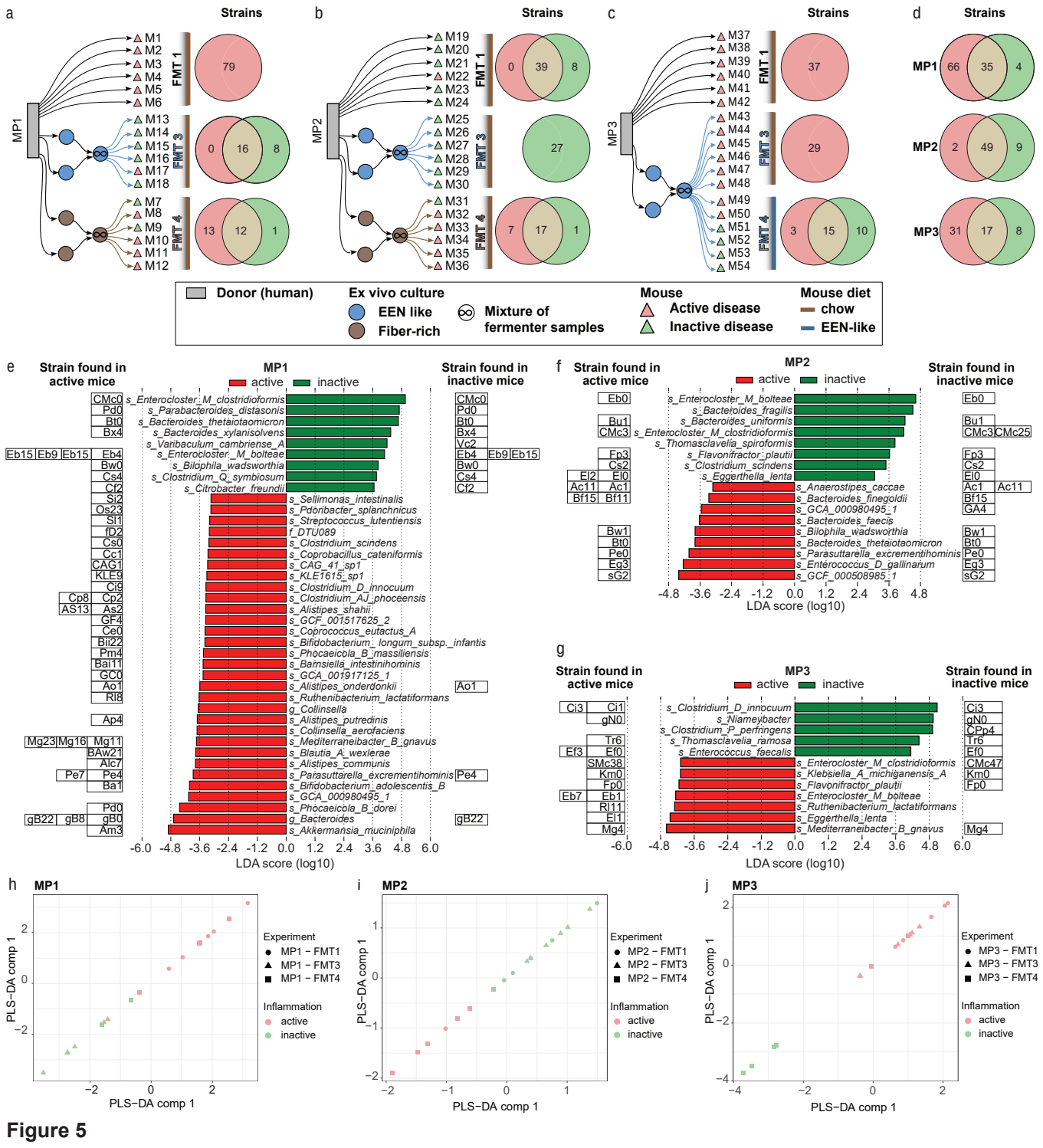
a
Strains
MP1
M1
M2
M3
M4
M5
M6
FMT 1
79
M13
M14
M15
M16
M17
M18
FMT 3
0
16
8
M7
M8
M9
M10
M11
M12
FMT 4
13
12
1
b
Strains
MP2
M19
M20
M21
M22
M23
M24
FMT 1
0
39
8
M25
M26
M27
M28
M29
M30
FMT 3
27
M31
M32
M33
M34
M35
M36
FMT 4
7
17
1
c
Strains
MP3
M37
M38
M39
M40
M41
M42
FMT 1
37
M43
M44
M45
M46
M47
M48
FMT 3
29
M49
M50
M51
M52
M53
M54
FMT 4
3
15
10
d
Strains
MP1
66
35
4
MP2
2
49
9
MP3
31
17
8
Donor (human)
Ex vivo culture
EEN like
Fiber-rich
Mixture of fermenter samples
Mouse
Active disease
Inactive disease
Mouse diet
chow
EEN-like
e
Strain found in active mice
MP1
active
inactive
Strain found in inactive mice
s_Enterocloster_M_clostridioformis
s_Parabacteroides_distasonis
s_Bacteroides_thetaiotaomicron
s_Bacteroides_xylanisolvens
s_Varibaculum_cambriense_A
s_Enterocloster_M_bolteae
s_Bilophila_wadsworthia
s_Clostridium_Q_symbiosum
s_Citrobacter_freundii
s_Sellimonas_intestinalis
s_Pdoribacter_splanchnicus
s_Streptococcus_lutentiensis
f_DTU089
s_Clostridium_scindens
s_Coprobacillus_cateniformis
s_CAG_41_sp1
s_KLE1615_sp1
s_Clostridium_D_innocuum
s_Clostridium_AJ_phoceensis
s_Alistipes_shahii
s_GCF_001517625_2
s_Coprococcus_eutactus_A
s_Bifidobacterium_longum_subsp._infantis
s_Phocaeicola_B_massiliensis
s_Barnsiella_intestinihominis
s_GCA_001917125_1
s_Alistipes_onderdonkii
s_Ruthenibacterium_lactatiformans
g_Collinsella
s_Alistipes_putredinis
s_Collinsella_aerofaciens
s_Mediterraneibacter_B_gnavus
s_Blautia_A_wexlerae
s_Alistipes_communis
s_Parasuttarella_excrementihominis
s_Bifidobacterium_adolescentis_B
s_GCA_000980495_1
s_Phocaeicola_B_dorei
g_Bacteroides
s_Akkermansia_muciniphila
LDA score (log10)
f
Strain found in active mice
MP2
active
inactive
Strain found in inactive mice
s_Enterocloster_M_bolteae
s_Bacteroides_fragilis
s_Bacteroides_uniformis
s_Enterocloster_M_clostridioformis
s_Thomasclavelia_spiroformis
s_Flavonifractor_plautii
s_Clostridium_scindens
s_Eggerthella_lenta
s_Anaerostipes_caccae
s_Bacteroides_finegoldii
s_GCA_000980495_1
s_Bacteroides_faecis
s_Bilophila_wadsworthia
s_Bacteroides_thetaiotaomicron
s_Parasuttarella_excrementihominis
s_Enterococcus_D_gallinarum
s_GCF_000508985_1
LDA score (log10)
g
Strain found in active mice
MP3
active
inactive
Strain found in inactive mice
s_Clostridium_D_innocuum
s_Niameybacter
s_Clostridium_P_perfringens
s_Thomasclavelia_ramosa
s_Enterococcus_faecalis
s_Enterocloster_M_clostridioformis
s_Klebsiella_A_michiganensis_A
s_Flavonifractor_plautii
s_Enterocloster_M_bolteae
s_Ruthenibacterium_lactatiformans
s_Eggerthella_lenta
s_Mediterraneibacter_B_gnavus
LDA score (log10)
h
MP1
PLS−DA comp 1
Experiment
MP1 − FMT1
MP1 − FMT3
MP1 − FMT4
Inflammation
active
inactive
i
MP2
PLS−DA comp 1
Experiment
MP2 − FMT1
MP2 − FMT3
MP2 − FMT4
Inflammation
active
inactive
j
MP3
PLS−DA comp 1
Experiment
MP3 − FMT1
MP3 − FMT3
MP3 − FMT4
Inflammation
active
inactive

Figure 5

643 ***Fig. 5: Individual species and strain signatures in recipient Il10$^{-/-}$ mice***

644 ***a-c*** *Transfer overview of donor sample (grey) from FMT 1 (black), FMT 3 (EEN-conditioned, blue) and FMT 4 (FR-*
645 *conditioned, brown) into Il10$^{-/-}$ mice. Mouse inflammation end-points are shown (triangles, red = active, green =*
646 *inactive). Venn diagrams tally strains detected in inflamed (red), non-inflamed (green) Il10$^{-/-}$ mice or found in both*
647 *conditions (yellow) for* ***a*** *MP1* ***b*** *MP2* ***c*** *MP3.* ***d*** *Venn diagrams combining strains across FMT1, 3, and 4 for each*
648 *MP.* ***e-g*** *LEfSe (Linear discriminant analysis Effect Size) analysis of differentially abundant bacteria at species level*
649 *based on metagenomic data in the recipient inflamed (active, red) or non-inflamed (inactive, green) Il10$^{-/-}$ mice with*
650 *abundance of strains in each condition. Different strains are labeled with different numbers.* ***e*** *MP1.* ***f*** *MP2.* ***g*** *MP3.*
651 ***h-j*** *Analyses of untargeted metabolomics with representative sPLS-DA plots comparing inflammation in*
652 *Il10$^{-/-}$ mice (inflamed = red; not inflamed = green) from FMT 1, 3 and 4. Axes indicate the sPLS-DA component*
653 *separating the groups.* ***h*** *MP1.* ***i*** *MP2.* ***j*** *MP3. Strain abundance cut-off 20%, species abundance cut-off 10^{-5},*
654 *prevalence ≥ 1.*

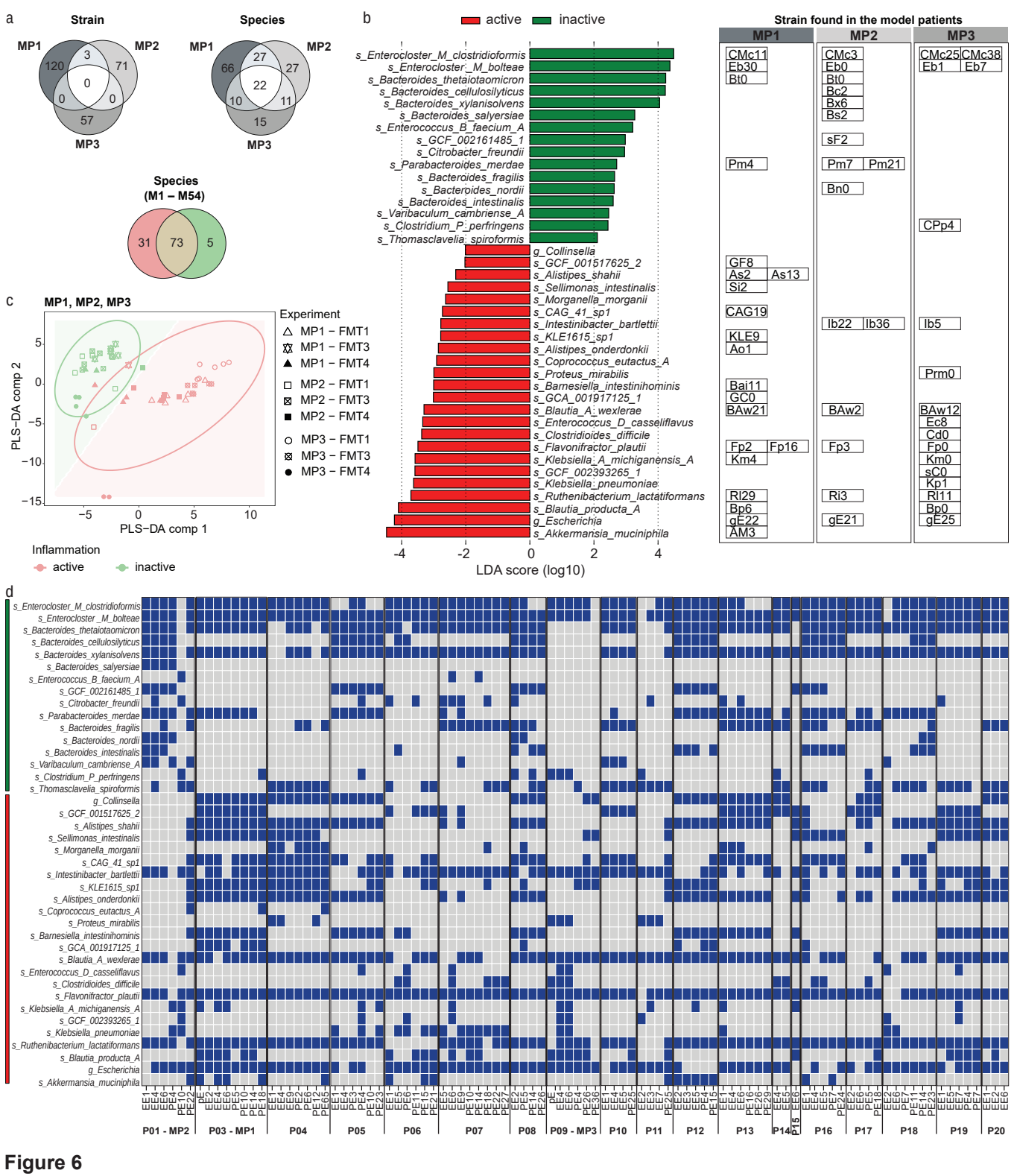
a
Strain
MP1
MP2
MP3
120
3
71
0
0
0
57
Species
MP1
MP2
MP3
66
27
27
22
10
11
15
Species
(M1 – M54)
31
73
5
b
active
inactive
s_Enterocloster_M_clostridioformis
s_Enterocloster_M_bolteae
s_Bacteroides_thetaiotaomicron
s_Bacteroides_cellulosilyticus
s_Bacteroides_xylanisolvens
s_Bacteroides_salyersiae
s_Enterococcus_B_faecium_A
s_GCF_002161485_1
s_Citrobacter_freundii
s_Parabacteroides_merdae
s_Bacteroides_fragilis
s_Bacteroides_nordii
s_Bacteroides_intestinalis
s_Varibaculum_cambriense_A
s_Clostridium_P_perfringens
s_Thomasclavelia_spiroformis
g_Collinsella
s_GCF_001517625_2
s_Alistipes_shahii
s_Sellimonas_intestinalis
s_Morganella_morganii
s_CAG_41_sp1
s_Intestinibacter_bartlettii
s_KLE1615_sp1
s_Alistipes_onderdonkii
s_Coprococcus_eutactus_A
s_Proteus_mirabilis
s_Barnesiella_intestinihominis
s_GCA_001917125_1
s_Blautia_A_wexlerae
s_Enterococcus_D_casseliflavus
s_Clostridioides_difficile
s_Flavonifractor_plautii
s_Klebsiella_A_michiganensis_A
s_GCF_002393265_1
s_Klebsiella_pneumoniae
s_Ruthenibacterium_lactatiformans
s_Blautia_producta_A
g_Escherichia
s_Akkermansia_muciniphila
-4
-2
0
2
4
LDA score (log10)
Strain found in the model patients
MP1
MP2
MP3
CMc11
Eb30
Bt0
Pm4
GF8
As2
As13
Si2
CAG19
KLE9
Ao1
Bai11
GC0
BAw21
Fp2
Fp16
Km4
Rl29
Bp6
gE22
AM3
CMc3
Eb0
Bt0
Bc2
Bx6
Bs2
sF2
Pm7
Pm21
Bn0
Ib22
Ib36
BAw2
Fp3
Ri3
gE21
CMc25
CMc38
Eb1
Eb7
CPp4
Ib5
Prm0
BAw12
Ec8
Cd0
Fp0
Km0
sC0
Kp1
Rl11
Bp0
gE25
c
MP1, MP2, MP3
PLS−DA comp 2
PLS−DA comp 1
5
0
−5
−10
−15
−5
0
5
10
Experiment
MP1 − FMT1
MP1 − FMT3
MP1 − FMT4
MP2 − FMT1
MP2 − FMT3
MP2 − FMT4
MP3 − FMT1
MP3 − FMT3
MP3 − FMT4
Inflammation
active
inactive
d
P01 - MP2
P03 - MP1
P04
P05
P06
P07
P08
P09 - MP3
P10
P11
P12
P13
P14
P15
P16
P17
P18
P19
P20

Figure 6

655 ***Fig. 6: Strains associated with active or inactive disease in Il10$^{-/-}$ mice***:
656 ***a*** *Left Venn diagram shows shared or individual species detected in MP1, MP2 and MP3. Lower Venn diagram*
657 *shows shared (yellow) or individual species detected inflamed (red) or not inflamed (green) Il10$^{-/-}$ mice from FMTs*
658 *from MP1, MP2 and MP3. Right Venn diagram shows shared or individual strains detected in MP1, MP2 and MP3.*
659 ***b*** *LEfSe (Linear discriminant analysis Effect Size) analysis of differentially abundant bacteria at species level in all*
660 *recipient inflamed (active, red) or non-inflamed (inactive, green) Il10$^{-/-}$ mice from all FMTs performed with abundance*
661 *of strains in each MP. Different strains are labeled with different numbers.* ***c*** *Visualization of inflamed and non-*
662 *inflamed mice on the two identified sPLS-DA components.* ***d*** *Abundance of differentially abundant strains from* ***b*** *in*
663 *all CD-EEN patients (blue = abundant, grey = not detected). Strain abundance cut-off 20%, species abundance cut-*
664 *off 10^{-5}, prevalence ≥ 1.*

665 **Online Methods**

666 **Patient cohort, recruitment and study design**

667 Patients (aged 3-18 years) with suspected or established IBD were recruited to a monocentric
668 pediatric IBD cohort study (ethics approval Ludwig-Maximilians University of Munich, approval
669 No. 17-801 and German Clinical Trials Register Accession No. DRKS00013306, date
670 registration 19.03.2018). All patients and parents/legal guardians provided written informed
671 consent/assent. Patients without confirmed IBD after full diagnostic work-up according to
672 revised Porto criteria were excluded[37]. All other patients were followed prospectively for one
673 year and treated according to current ESPGHAN/ECCO guidelines for CD or ulcerative colitis
674 (UC)/IBD unclassified (IBDU) [6,38,39]. Disease activity, as well as endoscopic, histologic,
675 radiologic and laboratory findings were collected prospectively. Disease activity indices
676 included the Physician Global Assessment (PGA) and the weighted pediatric Crohn's disease
677 activity index (wPCDAI) for CD, as well as the pediatric ulcerative colitis activity index (PUCAI)
678 for UC/IBDU. For EEN-treated CD patients, remission was defined as wPCDAI of <12.5 points
679 and response as reduction in wPCDAI of >17.5 points, but not reaching remission. Relapse
680 was defined as increase of wPCDAI to ≥12.5 points and/or fecal calprotectin of >250 mg/L
681 requiring changes in medical treatment or abdominal surgery or reintroduction of
682 EEN. Patients received detailed instructions for fecal specimen collections and time points, as
683 well as stool collection kits. Each sample was accompanied with a questionnaire on date and
684 time of specimen collection, problems during sampling, Bristol stool scale and recent antibiotic
685 use.

686 EEN therapy was prescribed for 6-8 weeks, followed by gradual re-introduction of solid food
687 and concomitant start of maintenance treatment. EEN was performed with Modulen® IBD
688 (Nestlé Health Science) or in case of intolerance (e.g. cow's milk protein allergy) with Neocate
689 Junior® (Nutricia, Erlangen, Germany). The amount of prescribed formula was based on the
690 Daily Recommendations Intake (DRI) using the online calculator:
691 https://www.nal.usda.gov/human-nutrition-and-food-safety/dri-calculator. All EEN-treated
692 patients received dietary advice and dietetic support to comply with complete liquid formula
693 feeding.

694 **Fecal specimen collection**

695 Samples were collected at home or in the hospital. Patients provided samples at baseline
696 (before bowel preparation for endoscopy) and every four weeks in (1) 4 mL DNA stabilizer
697 (magiX PBI Microbiome Preservation Buffer, microBIOMix GmbH, Regensburg)[40], (2) 8 mL
698 20% glycerol in reduced phosphate-buffered saline (PBS, 0.05% L-cysteine) and (3) naïve
699 without stabilizing solution. Patients on EEN collected stool in (1) weekly for the first 12 weeks.

700 Samples in (1) were shipped at ambient temperature by mail to the study center. Fecal
701 specimens in (2) and (3) were immediately frozen at home (approx. -18 to -20°C) and brought
702 in on wet ice packs at the next visit. Upon receipt, samples were aliquoted, barcoded, linked
703 to clinical data with CentraXX Bio (Kairos GmbH) and stored immediately at -80°C until further
704 analysis.

705 **Selection of donor samples for transfer experiments into germ-free mice**

706 Stool samples for FMT experiments into germ-free (GF) mice were selected according to the
707 following criteria: active disease included samples from treatment-naive patients before the
708 start of EEN (PreEEN), EEN-induced remission (EEN) or reintroduction of a regular diet
709 (PostEEN).

710 **Animal ethics statement**

711 All animal experiments were conducted at Technical University of Munich and approved by the
712 Committee on Animal Health Care and Use of the State of Upper Bavaria (TVA ROB-55.2-
713 2532.Vet_02-19-190) and performed in strict compliance with the EEC recommendations for
714 the care and use of laboratory animals (European Communities Council Directive of November
715 24, 1986 (86/609/EEC).

716 **Animals and housing conditions**

717 GF wild-type (WT) and *Il10*-deficient (*Il10*$^{-/-}$) mice on 129Sv/Ev background were bred and kept
718 at the Core Facility Gnotobiology of the ZIEL Institute for Food & Health, Technical University
719 of Munich, Freising, Germany. Mice were housed as described elsewhere[17], but using single
720 gnoto-cage units (Isocage P System, Tecniplast, Italy). Cages are ventilated with HEPA-
721 filtered air at 22 ± 1°C with a 12-h light/dark cycle. Female and male mice were assigned
722 randomly to the treatment groups with a ratio of 1:1 and six mice per genotype. Mice received
723 standard chow (V1124-300; Ssniff, Soest, Germany; autoclaved) or an EEN-like purified diet
724 (EEN-like, SNIFF S5745-E902, Supplement Fig. 1D) and sterile water *ad libitum*. EEN-like diet
725 was introduced one week prior to fecal microbial transfer (FMT) to allow for adaptation.
726 Handling of mice in isocages was performed under biological safety cabinets in sterile
727 conditions.

728 **Preparing gavage for humanizing germ-free mice**

729 Preparation of FMT with human fecal microbiota was performed according to Metwaly *et al*.
730 (2020)[17]. For post *ex vivo* FMT, frozen samples in glycerol (20% end concentration) were
731 thawed on ice. All steps were performed in an anaerobic chamber (90% N_2 and 10% H_2). *Ex*
732 *vivo* suspensions (2 mL) were centrifuged at 100×*g* for 3 min at 4°C to pellet debris.
733 Supernatant was collected and centrifuged at 8000×*g* for 10 min at 4°C to pellet the bacteria.
734 The bacterial pellet was resuspended in 1.5 mL reduced PBS (0.05% L-cysteine-HCl). The

735 clear supernatant was transferred into an anaerobic crimped tube, which was transferred to
736 the gnotobiotic facility. All mice were gavaged on three consecutive days and sacrificed after
737 four weeks of colonization (12 weeks of age).

738 **Tissue Staining and scoring**

739 Colonic and cecal Swiss-roll tissues were fixed, stained and scored as described before[17]. In
740 brief, tissue was fixed in 4% formaldehyde/PBS for 48 h at room temperature, subsequently
741 dehydrated (Leica TP1020), and embedded in paraffin (McCormick; Leica EG1150C).
742 Formalin-fixed paraffin-embedded (FFPE) tissue sections were stained with hematoxylin and
743 eosin (H&E) and scored 0 (not inflamed) to 12 (highly inflamed). Inflammation cut off was
744 defined as a histopathology score greater than three based on scoring in WT mice.

745 **Gene expression**

746 Tissue sections from colon were collected in RNAlater (Sigma Aldrich) for 24 h at 4°C and long-
747 term at -80 °C until processing. Total RNA from tissue was isolated by using the NucleoSpin
748 RNA II kit (Macherey-Nagel GmbH) according to manufacturer's instructions. Complementary
749 DNA was synthetized from 500 ng total RNA by using random hexamers and moloney murine
750 leukemia virus (M-MLV) reverse transcriptase (RT) Point Mutant Synthesis System (Promega).
751 Quantification was performed by using the LightCycler 480 Universal Probe Library System
752 (Roche Primers and probes used were: *Gapdh* (glyceraldehyde 3-phosphate dehydrogenase)
753 (5'-tccactcatggcaaattcaa-3´; 5' tttgatgttagtggggtctcg-3´; Probe #9) and *Tnf* (Tumor necrosis
754 factor) (5´-tgcctatgtctcagcctcttc 3´; 5´-gaggccatttgggaacttct-3´; Probe #49). Relative induction
755 of gene mRNA expression was calculated based the 2-ΔΔCt method [41] using the expression
756 of *Gapdh* for normalization.

757 ***Ex vivo* gut chemostat model**

758 The *ex vivo* continuous fermentation was performed in 1.4-L bioreactors (Multifors 2) and
759 monitored with Eve®software (Infors AG, Basel, Switzerland). Parameters were set as
760 described before[42]. Briefly, vessels were maintained at 37°C, pH 6.8 with a constant influx of
761 N_2 to maintain an anaerobic atmosphere. Inoculation material was prepared in an anaerobic
762 chamber (90% N_2 and 10% H_2). Approximately 2.5 g of frozen fecal samples was suspended
763 in reduced PBS supplemented with 0.03 g/mL L-cysteine-HCl, filtered (70 µm Cell Strainer,
764 FisherScientific) and evenly distributed between two vessels, which led to about 1.0×10^8 to
765 8.16×10^8 CFU/vessel. Two consecutive batch fermentations (24 h in 400 mL, another 24 h
766 with fresh 400 mL medium added) allowed fecal microbial communities to establish.
767 Continuous fermentation included complete medium exchange every 36 h (retention time) with
768 a working volume of 400 mL. After 10 days of continuous fermentation, where stable
769 community formation was achieved, samples for transfer into GF mice were collected and

770 medium was switched afterwards. After 1.5 days of complete medium exchange from medium
771 1 to medium 2, samples for transfer into mice were collected on day 9 of continuous
772 fermentation in the second medium. Medium composition was either fiber-rich (FR) or EEN-
773 like, mimicking patient conditions at sampling (PreEEN and PostEEN, respectively; **Extended**
774 **Data Fig.1a-e**).

775 FR medium was prepared according to Macfarlane *et al*. (1998)[43], but supplemented with
776 additional vitamins (pantothenate 10 mg/L, nicotinamide 5 mg/L, thiamine 4 mg/L, biotin 2
777 mg/L, vitamin B12 0.5 mg/L, menadione 1 mg/L, and p-aminobenzoic acid 5 mg/L) as
778 described in Gibson and Wang[44]. EEN-like medium was based on the Macfarlane medium, but
779 with modifications simulating colonic-luminal content during an EEN diet. To determine the
780 carbohydrate:protein ratio of digested Modulen IBD® in the colon, similar calculations as
781 described previously were conducted[45,46]. Since Modulen IBD® lacks fibers, these ingredients
782 present in the FR medium (i.e., pectin from citrus, guar gum, xylan from oat spelt, inulin from
783 *Dahlia* tubers, and arabinogalactan from larch wood) were replaced by soluble rice starch and
784 simple sugars. A total carbohydrate concentration of 13 g/L was chosen in alignment with
785 Cinquin *et al.* (2004)[45]. As the formulation of Modulen IBD® is not publicly available, we
786 decided to include some Modulen IBD® not to miss crucial nutrients in our model-colon
787 medium. Towards this end, 10% v/w of Modulen IBD® was added to the EEN-like medium.
788 Finally, the carbohydrate:protein ratio was 75:25 in the model medium. To further mimic
789 Modulen IBD®, casein was used as main protein source with the exclusion of tryptone and
790 peptone (**Supplement Fig. 1a-c**).

791 Samples were aseptically collected daily at the same daytime and stored at -80°C until further
792 analyses. Samples for transfer into the GF mice were collected and mixed with glycerol (20%
793 end concentration) and stored at -80°C until gavage preparation. In order to diminish potential
794 vessel effects in the technical duplicates of each fermenter colonization, samples from both
795 vessels were mixed 50:50 for gavage.

796 **High-throughput 16S-ribosomal RNA (rRNA) gene amplicon sequencing analysis**

797 Total DNA from human stool, colonic mouse content and the continuous *ex vivo* fermentation
798 was isolated using bead beating and sequenced for 16S rRNA gene amplicons as described[47].
799 Downstream analysis was performed in R v4.2.1 using Rhea
800 (https://lagkouvardos.github.io/Rhea/)[48]. zOTU tables were normalized to 10.000 reads, beta-
801 diversity was computed using generalized UniFrac distances[49]. Alpha-diversity was assessed
802 on the basis of taxa richness and Shannon effective number of zOTUs[50]. Trees were visualized
803 and annotated using EvolView (http://www.evolgenius.info/evolview/)[51]. Differential analyses
804 of bacteria in different groups was done using LDA Effect Size (LEfSe)[52]. zOTUs were re-

805 checked using the 16S-based ID tool of EzBioCloud[69] using the database update 2023.08.23,
806 reflecting all taxa published and accepted by IJSEM until April 2023.

807 **Shotgun Metagenomic Sequencing and Analysis**

808 Metagenomic sequencing was performed for 96 human stool samples and 66 samples from
809 transfer experiments (54 mouse, 12 *ex vivo*) using the genomic DNA already isolated for 16S
810 rRNA gene amplicon sequencing. DNA was randomly sheared into short fragments. The
811 obtained fragments were end repaired, A-tailed, and further ligated with Illumina adapters. The
812 fragments with adapters were size-selected, PCR amplified, and purified. The library was
813 checked with Qubit and real-time PCR for quantification and BioAnalyzer for size distribution
814 detection as required by Illumina (TruSeq® DNA Library Prep Kit). Quantified libraries were
815 pooled and sequenced on a NovaSeq platform (Illumina) in PE150 mode. Raw data were
816 aimed at 15 Gb per demultiplexed sample. From raw shotgun metagenomic sequencing data,
817 adapter sequences were removed using Trimmomatic v0.39[53] without considering any
818 mismatch and parameters LEADING:3, TRAILING:3, and SLIDINGWINDOW:4:15. We
819 removed human reads by mapping against human reference genome hg38 by using Bowtie2
820 v2.4.5 [54] with the default parameters. Cleaned fastq data files were used in the following steps.

821 Strain tracking and strain gene content analyses were performed based on the StrainPGC
822 workflow [@Smith2023, https://github.com/bsmith89/StrainPGC]. Briefly, preprocessed
823 metagenomes were metagenotyped using GT-Pro v1.0.1[55]. Across all samples, 369 species -
824 as defined in the Unified Human Gut Genome (UHGG)[56] - were robustly detected and only
825 these were included in downstream pangenome profiling. Single nucleotide polymorphism
826 (SNP) profiles were filtered, subsampled, and strain relative abundances were estimated with
827 StrainFacts v0.4.0[16]. Within individual species, estimated strain fractions add up to 100%. By
828 contrast, other analyses considered the overall strain composition: the relative abundance of
829 each strain across all species.

830 Gene profiling was performed against a subset of the MIDASDB-UHGG pangenome database
831 v.15[57] dereplicated at a 99% ANI threshold performed and mapping reads using Bowtie2
832 v2.4.5[54]. Species abundances were estimated based on the average depth of core genes.
833 Global functional gene family profiling was performed by aggregating gene depths into Clusters
834 of Orthologous Genes (COGs) across all species and then normalizing based on 25 ubiquitous,
835 single-copy genes to estimate “gene copies per genome”.

836 **Metabolomics**

837 **Sample preparation / Metabolites extraction**

838 **Sample preparation of mouse colon content.** Approximately 20 mg of mouse colon content
839 was weighed in a 2 mL bead beater tube (FastPrep-Tubes, Matrix D, MP Biomedicals Germany

840 GmbH, Eschwege, Germany). Next, 1 mL of methanol-based dehydrocholic acid extraction
841 solvent (c = 1.3 µmol/L) was added as an internal standard for work-up losses. The samples
842 were extracted with a bead beater FastPep-24TM 5G (MP Biomedicals Germany GmbH,
843 Eschwege, Germany) supplied with a CoolPrepTM (MP Biomedicals Germany, cooled with dry
844 ice) 3-times each for 20 s of beating at a speed of 6 m/s and followed by a break of 30 s each.
845 **Sample preparation of fermenter or human samples.** Either 200 mg of the fermenter
846 samples or 100 mg of human fecal samples was weighed in a 15 mL bead beater tube
847 (FastPrep-Tubes, Matrix D, MP Biomedicals Germany GmbH, Eschwege, Germany). Next,
848 5 mL of methanol-based dehydrocholic acid extraction solvent (c = 1.3 µmol/L) was added as
849 an internal standard for work-up losses. The samples were extracted with the same FastPrep
850 protocol described above.
851 **Targeted bile acid measurement.** A standard of 20 µL of isotopically labeled bile acids (ca. 7
852 µM each) were added to 100 µL of sample extract. Targeted bile acid measurement was
853 performed using a QTRAP 5500 triple quadrupole mass spectrometer (Sciex, Darmstadt,
854 Germany) coupled to an ExionLC AD (Sciex, Darmstadt, Germany) ultrahigh performance
855 liquid chromatography system. A multiple reaction monitoring (MRM) method was used for the
856 detection and quantification of the bile acids according to Reiter et. al.[58] Data acquisition and
857 instrumental control were performed with Analyst v1.7 software (Sciex, Darmstadt, Germany).
858 **Untargeted mass spectrometric measurement.** The untargeted analysis was performed
859 using a Nexera UHPLC system (Shimadzu, Duisburg, Germany) coupled to a Q-TOF mass
860 spectrometer (TripleTOF 6600, AB Sciex, Darmstadt, Germany). Separation of the fecal
861 samples was performed either using a UPLC BEH Amide 2.1 × 100 mm, 1.7 µm analytic
862 column (Waters, Eschborn, Germany) with a 400 µL/min flow rate or with a Kinetex XB18 2.1
863 x 100 mm, 1.7 µm (Phenomenex, Aschaffenburg, Germany) with a 300 µL/min flow rate. For
864 the HILIC-separation the settings were as follows: The mobile phase was 5 mM ammonium
865 acetate in water (eluent A) and 5 mM ammonium acetate in acetonitrile/water (95/5, v/v) (eluent
866 B). The gradient profile was 100% B from 0 to 1.5 min, 60% B at 8 min and 20% B at 10 min to
867 11.5 min and 100% B at 12 to 15 min. For the reversed-phase separation, eluent A was 0.1%
868 formic acid and eluent B was 0.1% formic acid in acetonitrile. The gradient profile started with
869 0.2% B which was held for 0.5 min. Afterwards, the concentration of eluent B was increased
870 to 100% until 10 min which was held for 3.25 min. Subsequently, the column was equilibrated
871 at starting conditions. A volume of 5 µL per sample was injected. The autosampler was cooled
872 to 10 °C and the column oven heated to 40 °C. Every tenth run, a quality control (QC) sample,
873 which was pooled from all samples, was injected. The samples were measured in a
874 randomized order and in the Information Dependent Acquisition (IDA) mode. MS settings in
875 the positive mode were as follows: Gas 1 55, Gas 2 65, Curtain gas 35, Temperature 500 °C,
876 Ion Spray Voltage 5500, declustering potential 80. The mass range of the TOF MS and MS/MS

877 scans were 50–2000 m/z and the collision energy was ramped from 15–55 V. MS settings in
878 the negative mode were as follows: Gas 1 55, Gas 2 65, Cur 35, Temperature 500 °C, Ion
879 Spray Voltage -4500, declustering potential -80. The mass range of the TOF MS and MS/MS
880 scans were 50–2000 m/z and the collision energy was ramped from -15–55 V.

881 **Data processing**

882 The "msconvert" from ProteoWizard[59] was used to convert raw files to mzXML (de-noised by
883 centroid peaks). The bioconductor/R package xcms[60] was used for data processing and
884 feature identification. More specifically, the matchedFilter algorithm was used to identify peaks
885 (full width at half-maximum set to 7.5 s). Then the peaks were grouped into features using the
886 "peak density" method[60]. The area under the peak was integrated to represent the abundance
887 of features. The retention time was adjusted based on the peak groups presented in most
888 samples. To annotate features with names of metabolites, the exact mass and MS2
889 fragmentation pattern of the measured features were compared to the records in HMBD[61] and
890 the public MS/MS spectra in MSDIAL[62], referred to as MS1 and MS2 annotation, respectively.
891 Missing values were imputed with half of the limit of detection (LOD) methods, i.e., for every
892 feature, the missing values were replaced with half of the minimal measured value of that
893 feature in all measurements. To confirm a MS2 spectra is well annotated, we manually
894 reviewed our MS2 fragmentation pattern and compared it with records in the public database,
895 previously measured reference standards and SIRIUS[63] to evaluate the correctness of the
896 annotation. Significances of well-annotated metabolic features were computed with analysis
897 of variance (ANOVA) per donor or Wilcoxon signed-rank tests and FDR-corrected using the
898 Benjamin-Hochberg method for three donors. Subsequent hierarchical clustering using only
899 differentially abundant metabolites ($q < 0.05$) was conducted using complete linkage based on
900 Euclidean distances. Calculations, as well as heatmaps, were computed in R v4.2.1. For each
901 principal component analysis (PCA), we included negative and positive features from RP and
902 HILIC with at least 50% non-missing values per condition (inflamed/non-inflamed). The
903 remaining missing values were imputed as described above. The prcomp function from R
904 v4.3.2 computed the principal components after centering and scaling each feature to zero
905 mean and unit variance. Sparse Partial Least Squares Discriminant Analysis (sPLS-DA) was
906 performed on centered and scaled features using the mixOmics bioconductor/R package
907 v6.26.0[64]. Mean balanced error rate, was used to select the number of components and
908 features in M-fold cross-validation where M corresponds to the minimum number of samples
909 per condition. **Extended Data Fig. 5e** shows raw values for features with the highest Variable
910 Importance in the Projection (VIP), i.e., features contributing the most to explaining the
911 conditions.

912

913 **Data integration of 16s rRNA amplicon data with metabolomics and metagenomics**

914 We matched 60 samples from 15 patients of the 16S-rRNA gene sequencing to 60 samples of
915 the untargeted metabolomics analysis according to patient ID and same time points. The aim
916 was to discriminate features between 23 EEN samples (clinical phenotype mild and remission)
917 and 37 PostEEN samples (>2 weeks after EEN, clinical remission). For the integrated selection
918 of metabolome and microbiota features, sPLS-DA (mixOmics v6.20) was used[64]. For feature
919 selection concerning metabolomics, only annotated metabolites were considered. As
920 described above, input metabolites were mean-centered and scaled to unit variance. zOTUs
921 (zero-radius operational taxonomic units) were centered log-ratio transformed. To estimate the
922 degree of overfitting, the model was trained on 70% of the data, with a k-fold cross-validation
923 for feature selection during training. The remaining 30% of the data were used to evaluate the
924 generalization power. The model performance was measured with an Area Under the Receiver
925 Operating Characteristic (ROC-AUC). This procedure was done once with the actual labels
926 and 200-times with randomized labels, to obtain an empirical p-value for the model prediction
927 on the validation data. Subsequently, Spearman's rank correlation coefficients between all
928 selected metabolites and zOTUs were computed and their respective p-values were corrected
929 with the Benjamini-Hochberg procedure[65]. All coefficients with an FDR >0.05 were set to 0.
930 Using all non-zero correlations, a network was generated and the Louvain method for
931 community detection[66] was applied to extract highly connected subgraphs from the correlation
932 network. For each community, a sPLS-DA model was trained with the same train-test and
933 randomization scheme explained previously for feature selection. Feature importance was
934 plotted using the loadings in each iteration and determining their association to either EEN or
935 PostEEN. Analyses were run in R v4.2.1 and python v3.8.11. For network analysis the igraph
936 v1.3.4[67] and networkx v3.1[68] packages were used.

937 Profiles of 16S rRNA amplicon relative abundance were further integrated with metagenomic
938 species profiles in order to identify those which represent the same, underlying taxa. This was
939 done by calculating the Pearson correlation coefficient between each zOTU relative
940 abundance and species relative abundances estimated from the metagenomic workflow. Each
941 correlation was then weighted by the mean relative abundance of that zOTU and species,
942 respectively, producing a matrix of matching scores for each comparison. Based on this score,
943 we ranked zOTUs for each species and species for each zOTU. We selected as putative
944 matches all zOTU-species pairs that were either reciprocal best hits or a combination of one
945 best hit and one second-best hit. In this way, we accounted for the possibility of multiple zOTUs
946 representing a species or multiple species being represented by a zOTU.

947 **Statistical analysis**

948 Further statistical analyses and plots were generated using GraphPad Prism v8.0 (GraphPad,
949 La Jolla, CA) using Mann-Whitney test, ANOVA followed by pairwise comparison testing

950 (Tukey, Bonferroni correction), by Kruskal-Wallis test followed by Dunn`s multiple comparisons.
951 Data is presented as mean ± SD. P-values below 0.05 were considered significant ($p < 0.05$,
952 *; $p < 0.01$, **; $p < 0.001$, ***; and $p < 0.0001$, ****).

953 Taxonomic turnover in both zOTU and strain compositions were calculated based on the Bray-
954 Curtis dissimilarity. Pairs where one sample was collected during EEN and the other during
955 PostEEN were classified as "transition". All within-subject pairwise comparisons were
956 computed and fit using cubic spline regression of the time between sample collections, with a
957 regression term for each subject, as well as for each pair class: EEN, transition, or PostEEN.
958 The null hypothesis of no difference between pair classes was tested by permutation: 999
959 random permutations of samples within subjects. Changes in mean, normalized, COG depths
960 during EEN and PostEEN time points were tested using the Wilcoxon signed-rank test across
961 subjects. False discovery rates were calculated using the Benjamini-Hochberg procedure.
962 Mean fold change for each COG was calculated as the ratio between these two estimates.

963 **Data availability**

964 The data that support the findings of this study will be available on reasonable request from
965 the corresponding author [TS]. The data are not publicly available due to the pediatric age of
966 the research participants. Mouse untargeted metabolomics data is available at Massive
967 (https://massive.ucsd.edu) under the number MSV000094047. All other data will be available
968 at the time of publication.

969

970 **Code availability**

971 Mutliomic data integration of 16S rRNA and metabolomics code is available at
972 https://doi.org/10.5281/zenodo.10808412. All code necessary to reproduce the metagenomic
973 data analysis will be made publicly available at the time of publication.